**Department of physics and astronomy**
**Heidelberg university**

Bachelor Thesis in Physics
submitted by

Amanda Camille Florig

born in Strasbourg (France)

**2023**

# Short light pulses and nonlinear interactions within a gas filled fiber

This Bachelor Thesis has been carried out by Amanda Camille Florig at the MPIK
Max-Planck Institute for nuclear physics in Heidelberg
under the supervision of
Dr. Christian Ott

# 1 Abstract

The field of short time spectroscopy is becoming increasingly relevant as the researched physical phenomena take place on smaller and smaller timescales.
This work deals with the generation of ultrashort laser pulses and their propagation through hollowcore fibers filled with noble gases, as well as related short-lived phenomena. First, I will introduce various concepts of optics such as dispersion, nonlinear medium response and some related nonlinear effects, for instance self-phase modulation or self-steepening.
Using hollowcore fibers is one of the most common approaches these days to compress short pulses. I will discuss the hollowcore fiber's pulse broadening and compression effect, and how they allow for the shortening of pulses from tens of femtoseconds to just a few femtoseconds. Then, I will introduce a numerical approach, the Split-Step Fourier method, to model and simulate the characteristics of such pulses. The simulation of the pulse's propagation will allow for a better visualization of the correlation of the pulse's and fiber's parameters. This includes for instance the pulse duration, spectral width, fiber pressure or which gas the fiber is filled with. The simulation will also allow me to present the influence of the previously mentioned nonlinear effects.
Finally, I will compare my numerically simulated data to experimental data measured at the MPIK and discuss the accuracy of the results.

# 2 Zusammenfassung

Kurzzeit Spektroskopie ist ein immer wichtiger werdendes Gebiet der Physik, da die erforschbaren Phänomene auf immer kleineren Zeitskalen stattfinden.
In dieser Arbeit sollen die Generierung und Ausbreitung von ultrakurzen Laserpulsen durch edelgasgefüllte Hohlfasern sowie damit zusammenhängende kurzlebige Phänomene diskutiert werden. Zuerst werde ich verschieden Begriffe der Optik, wie zum Beispiel Dispersion, nichtlineare Wechselwirkung mit Materie und damit verbundene nichtlineare Effekte, wie die Selbstphasenmodulation oder Selbstaufsteilung, einführen.
Hohlfasern sind eines der gängigsten Mittel um kurze Pulse zu komprimieren. Ich werde in dieser Arbeit auf ihren Verbreiterungs und Komprimiereffekt eingehen. Diese Effekte ermöglichen es, Pulse mit Dauern im Bereich von mehreren zehnen von Femtosekunden auf nur wenigen Femtosekunden zu verkürzen. Als nächstes werde ich die Split-Step Fourier Methode einführen, die es ermöglicht die Charakteristiken der Laserpulse in Hohlfasern numerisch zu approximieren. Die Simulation der Pulspropagation ist hilfreich, um die Korrelationen der Parameter des Pulses und der Faser besser zu verstehen. Unter diesen entscheidenden Parameter befinden sich zum Beispiel Pulsdauer, spektrale Breite, Faserdruck oder welches Füllgas benutzt wird. Durch die Simulation lässt sich unter Anderem auch der Einfluss der zuvor genannten nichtlinearen Effekte gut visualisieren.
Zum Schluss werde ich die numerischen Daten mit den in dem MPIK experimentell gemessenen Daten vergleichen und die Zuverlässigkeit der Ergebnisse bewerten.

# Contents

# 3 Introduction

Short time spectroscopy encompasses the investigation of dynamic processes in matter using spectroscopic means, for example light or more specifically, pulsed lasers. Currently, pulse durations of the magnitude of up to femto- or even attoseconds can be reached , allowing for the observation of processes in this time scale. In my thesis, I will discuss the workings of short pulse lasers and their propagation through hollowcore fibers. They grant the possibility to shorten laser pulses to up to a few or even single cycle regime.

The field of ultrafast optics was first pioneered in mode locking studies with solid-state and organic dye lasers as soon as the 1960s and early 1970s. [22] Lasers, which are characterized by their high coherence, monochromaticity and intensity, have been developed very far in their various applications ever since their development in the 60s. The generation of ultrashort laser pulses is a major field of research with a diversity of applications.

Since the invention of the pulsed laser, physicists have been trying to reduce the pulse duration further and further for two main reasons. Many fundamental processes in nature occur on very short time scales (pico- or femtosecond range). Performing time-resolved measurements of these processes requires ultrashort pulses. Furthermore, the peak power of the pulses increases with shorter pulse durations assuming constant energy.

This shortened pulse duration allows the investigation of the nonlinear interaction of high-intensity laser pulses within a medium. At present short intense lasers pulses are not only being used to study the fundamental physical interaction with matter, but are also already being applied for studying larger systems relevant in chemistry or biology. As many wide fields ermerged from their invention, Gérard Mourou and Donna Strickland received the Nobel Prize in physics "for their method of generating high-intensity, ultrashort optical pulses" [5] in 2018.

The method of chirped pulse amplification presently enables pulses that have a duration in the order of $10^1$ fs and an intensity in the order of $10^1$ mJ [22]. The pulse duration is typically limited by the broadness of the spectrum, which is itself restricted by the gain medium used in the specific laser.

In 1996, Nisoli et al [15] took advantage of the nonlinear interactions of pulses inside a gas-filled hollow fiber, which resulted in the pulses' spectral broadening. Henceforward the analysis of these nonlinear effects has continued advancing and producing wider spectral bandwidths. By compressing these high-energy laser pulses, it is now possible to achieve pulse durations of few femtoseconds. In this thesis, the linear and nonlinear behavior of short pulses inside of a hollowcore fiber filled with multiple noble gases will be examined.

Chapter 4 serves as an introduction to the subject matter of ultrashort laser pulses. First, the mathematical description of short pulses and their propagation in a hollowcore fiber is discussed. In the course of the section, the key terms which are necessary for the understanding of the work will be clarified. These include chromatic dispersion as well as nonlinear effects, most importantly self-phase modulation and self-steepening.

In chapter 5 the experimental setup is introduced, including a Ti:Sa laser which generates short intense laser pulses with a central wavelength at around 800 nm. The pulses are used to seed an optic parametric amplifier, enabling the generation of short pulses at variable wavelength ranges ($1.1-2.4$ $\mu$m). The latter are then focused into the hollowcore fiber for spectral broadening.

In chapter 6 the theoretical model used to describe the propagation of short intense pulses in a medium is introduced. The temporal and spectral evolution of short pulses is approximated by solving the generalized nonlinear Schrödinger equation, a computational task well known in quantum mechanics. As several efficient codes for numerical implementation freely shared as open source code were available, one task was to find the best working solution in order to compare the theory to the experiment or even to predict experimental results. Therefore the program Luna, written in the programming language Julia,

was chosen to process the main task of describing pulse propagation. Very high performances can be achieved with Julia. This is partially due to the option of using functions in Julia that are native to C. Julia's performance is also improved as it is a compiled language, meaning the code is translated into machine code, which is then directly executed.
The results from Luna can be saved and later compared using other simpler programming languages like Python or Matlab.
In chapter 7 I will show my results using Luna, demonstrating that all the important physical effects describing pulse propagation inside a hollowcore fiber can be implemented. Additionally, experimental data for pulse broadening in an argon and neon filled hollowcore fiber are presented and compared to simulations of similar input pulse parameters.

# 4 Physical basics

The following chapter introduces the fundamentals of physics which are relevant to later chapters, by first giving some basic relations of importance followed by the description of coherent short pulses in the time and frequency domain. Furthermore, the Gaussian beam is introduced as a possible spatial component of a focused light beam. Then, I will introduce the coupling and propagation properties of a hollowcore fiber, which are used to broaden the laser pulses in this work. Moreover, I will explain chromatic dispersion and multiple nonlinear effects applicable in order to modulate the spectral and temporal profile of short pulses.

## 4.1 Some light fundamentals

To understand the behavior of electromagnetic waves, the first fundamental relation one should take note of is:

$$E_\gamma \;=\; h \cdot f \;=\; \frac{h \cdot c}{\lambda} \tag{1}$$

with $E_\gamma$ being the energy of a photon, $h \;=\; 6.62607015 \cdot 10^{-34}\ \frac{m^2 \cdot kg}{s}$ the Planck constant, $f$ its frequency, $c$ the speed of light ($=\ 299792458\ \frac{m}{s}$in vacuum) and $\lambda$ its wavelength. $E_\gamma$ can be also written as follows, with $\omega$ being the angular frequency of the photon and $\hbar$ being equivalent to $\frac{h}{2\pi}$:

$$\omega \;=\; 2 \cdot \pi \cdot f \;\longrightarrow E_\gamma \;=\; \hbar \cdot \omega \tag{2}$$

When describing light, it is possible to do so using the wavelength or the frequency spectrum. Spectrum and spectral phase vary depending on whether they are shown in dependency of frequency or of wavelength. Thus it is important to know how the transformation between these two domains functions. The spectral phase $\phi$ can be transferred between wavelength and frequency spectrum as follows:

$$\phi_\lambda(\lambda) = \phi_\omega(2\pi c\frac{1}{\lambda}) \tag{3}$$

This relation can be derived from the definition of $\omega$ in equation 2 and the relation between $f$ and $\lambda$ from equation 1.
In order to transform the spectrum $S$, we must integrate it as follows:

$$\begin{aligned} &\int_{\infty}^{-\infty} S_\omega(2\pi c\frac{1}{\lambda})d\omega \\ &= \int_{-\infty}^{\infty} -S_\omega(2\pi c\frac{1}{\lambda})\frac{d\omega}{d\lambda}d\lambda \\ &= \int_{-\infty}^{\infty} S_\omega(2\pi c\frac{1}{\lambda})\frac{2\pi c}{\lambda^2}d\lambda \end{aligned} \tag{4}$$

Note that the energy doesn't change when integrating the spectrum over frequency as opposed to wavelength, as it is still the same spectrum.
This leads us to the conclusion:

$$S_\lambda(\lambda) = S_\omega(2\pi c\frac{1}{\lambda})\frac{2\pi c}{\lambda^2} \tag{5}$$

$\frac{2\pi c}{\lambda^2}$ is the Jacobi factor and is added due to the substitution in the integration. For now, I will mainly work with the frequency spectrum. However, using the wavelength spectrum will come in handy when comparing experimental results.
In order to conduct experiments with laser beams, it is essential to understand how to control their propagation through media. For instance, photons with different wavelengths propagate at different speeds,

which vary depending on the medium. One must also keep in mind that the spatial focusing can easily be compromised by any manipulation of the beam.

As light can be described as a wave, the Heisenberg uncertainty principle also applies to light beams.

$$\Delta E \Delta t \geq \frac{\hbar}{2} \tag{6}$$

$$\Delta \vec{p} \Delta \vec{x} \geq \frac{\hbar}{2} \tag{7}$$

$$E = \hbar\omega \quad \longrightarrow \Delta\omega \Delta t \geq \frac{1}{2} \tag{8}$$

$\Delta$ referring to the uncertainty of the subsequent variable, $\vec{p}$ being the momentum, $\vec{x}$ the location. In the case of a short light pulse, $\Delta t$ and $\Delta\omega$ refer tor the temporal and spectral width. Here inequality is a direct consequence of the the Fourier relation between the temporal and spectral field.

## 4.2 Short light pulses

The electric field $E$ of a coherent light pulse in vacuum can be used to describe short pulses mathematically. In the following formula, the spatial evolution and the vector character of $E$ is neglected to give us a simplified model:

$$E(t) \ = \ \frac{1}{2} A(t) e^{-i\phi(t)} + c.c. \tag{9}$$

$$\phi(t) = \phi_{CEP} + \omega_0 t + Ct^2 + \mathcal{O}(t^3) \tag{10}$$

$A$ is the real envelope of the pulse. A good example for such an envelope could be a Gaussian $A(t) = A_0 e^{-2log(2)\frac{t}{\tau_{FWHM}}^2}$, $\tau_{FWHM}$ being the full width half maximum (FWHM) of the temporal intensity profile

$$I(t) = \frac{c\epsilon_0}{2} \big\langle E_0(t) \big\rangle^2 \tag{11}$$

with c as the speed of light in vacuum and $\epsilon_0$ the vacuum permittivity.
Concerning the phase $\phi(t)$, the constant term describes the carrier envelope phase (CEP), which is responsible for shifting the carrier through time within the envelope. CEP effects usually only become relevant for laser pulses with very few cycles. The linear term contains the carrier frequency $\omega_0$. The quadratic term creates the chirp $C$ in time. As a result, a field with a positive chirp will oscillate more slowly at the beginning of the pulse and faster at the end. This becomes more apparent when looking at the derivative in time of equation10, as the *instantaneous frequency* $\frac{\partial\phi(t)}{\partial t}$ increases or decreases with time depending on the sign of $C$:

$$\frac{\partial\phi(t)}{\partial t} = \omega_0 + 2C \cdot t + \frac{\partial\mathcal{O}(t^3)}{\partial t} \tag{12}$$

A visualization of a typical unchirped and chirped pulse is presented in figure 1 and later in figure 2.

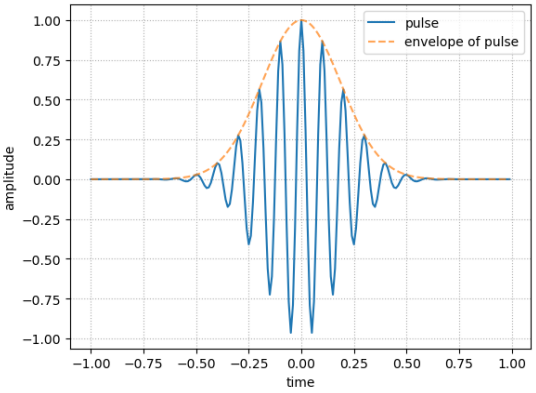


(a) Gaussian pulse with arbitrary units

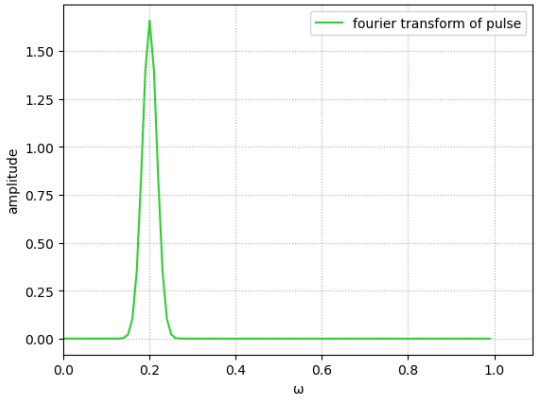


(b) Fourier transform of Gaussian pulse with arbitrary units

Figure 1

Unfortunately, it is currently impossible to measure the field in time due to the high speed at which the carrier oscillates and the slower response time of modern detectors. Hence, switching into the spectral domain by applying a Fourier transformation may be useful. We thus have two different ways to express electric fields mathematically:

$$E(t) \ = \mathcal{F}^{-1}[E(\omega)] = \ \frac{1}{2\pi}\int_{-\infty}^{+\infty} \tilde{E}(\omega)e^{i\omega t}\ dt \tag{13}$$

and the Fourier transform:

$$\tilde{E}(\omega) = \mathcal{F}[E(t)] \ = \ \int_{-\infty}^{+\infty} E(t)e^{-i\omega t}\ d\omega \tag{14}$$

Since the electric field is a real quantity, the Fourier transform $\tilde{E}(\omega)$ is hermitian, meaning that $\tilde{E}^*(\omega) = \tilde{E}(-\omega)$. For computational methods, it is useful to redefine the temporal electric field:

$$E(t) \ = \ \frac{1}{2}A(t)e^{i\omega_0 t} + c.c. \tag{15}$$

$$A(t) = \sqrt{\frac{2}{c\epsilon_0}I(t)} \cdot e^{i(\phi_{CEP}+Ct^2+\mathcal{O}(t^3))} \tag{16}$$

With the complex envelope $A(t)$, most important properties are included in the envelope and the carrier part ($e^{i\omega_0 t}$), which only results in a constant offset for the Fourier transformed frequency field. If the pulse length stays the same, but the individual frequency components arrive at different times, the central frequency will remain unchanged, but a much broader spectrum will be required to support such a short pulse duration. This is an example of a chirped pulse. It's most prominent characteristic is the pulse's instantaneous frequency change over time inside of the envelope. In the following example, the instantaneous frequency increases over time, which is referred to as an *up-chirp*. The corresponding spectrum of the chirped pulse is shown in figure 2b). It is noticeably broader than the spectrum of the unchirped pulse, as can be seen in figure 1b), despite the pulses having the same duration. In this example, the unchirped pulse is bandwidth-limited, meaning it has the shortest possible pulse duration for the corresponding spectral width. If it was to decrease instead, implying $C < 0$, the pulse would be called *down-chirped*. Generally, in case of a Gaussian envelope, the bandwidth-product $\Delta\omega \cdot \tau_{FWHM}$ is 0.44, $\Delta\omega$ being the full width half maximum of the Gaussian shaped spectrum.

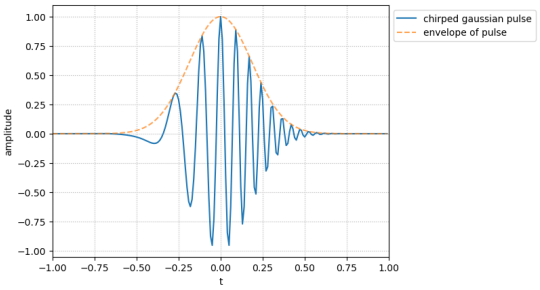


(a) chirped Gaussian pulse with arbitrary units

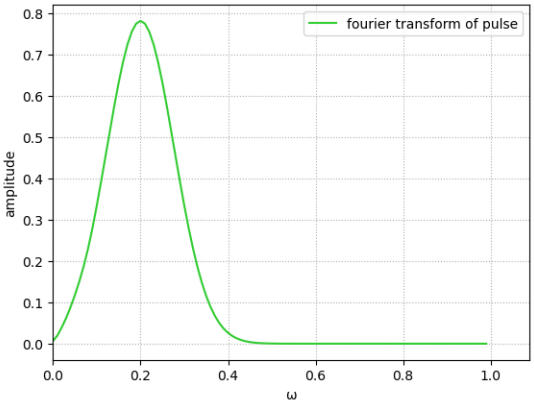


(b) Fourier transform of chirped Gaussian pulse with arbitrary units

Figure 2

## 4.3 Spatial component

Gaussian optics are a useful way of describing monocromatic light beams. Up until now, we only considered the temporal component of light. I will now give an example of its spatial component.
Ordinarily, in experiments, coherent light is generated through lasers. In the simplest case, the emitted collimated beam can be defined as a plane wave in space with an additional factor of $e^{\pm ik_z z}$ to the complex component of the field (see equation 9). On a more sophisticated level, the propagation of a laser beam can be expressed using Gaussian optics.
The intensity profile of a Gaussian beam focused at $z = 0$ can be described as follows:

$$I(r,z) \;=\; I_0 \cdot \left(\frac{w_0}{w(z)}\right)^2 \cdot \exp\left\{-\frac{2r^2}{\omega(z)^2}\right\} \tag{17}$$

with $I$ being the intensity, $I_0$ the peak intensity, $w$ the beam waist, $w_0$ the beam waist radius in the focus, $z$ the position along the beam axis and $r$ the distance from the aforementioned axis. The divergence angle $\theta$ is the angle at which the beam waist expands along the $z$-axis with

$$\theta \;=\; \frac{\lambda}{w_0 \pi} \tag{18}$$

In the case of a non-tight focus, meaning a long focal length $l_f$, the beam waist $w_0$ can be approximated as follows:

$$w_0 \;=\; \frac{\lambda}{2\pi \cdot tan\left(\frac{w(l_f)}{l_f}\right)} \;=\; \frac{\lambda \cdot l_f}{2\pi \cdot w(l_f)} \tag{19}$$

$\omega(l_f)$ is the beam waist at the position of the focusing optic.
The result is a distribution of intensity of this aspect:

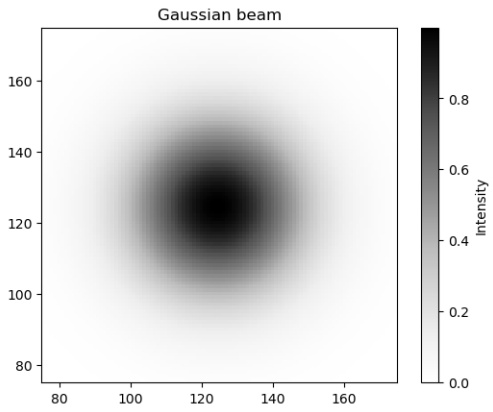


Figure 3: Intensity profile of Gaussian beam cross-section, arbitrary units

## 4.4 Hollowcore fiber

A hollowcore fiber is an optical fiber used for guiding light. In our case, we are using a hollowcore fiber that can be filled with a noble gas like argon. With a refractive index between about $1.4 - 1.5$, the *cladding* of the fiber (outer material), being fused silica, is slower for light to travel in than *core* (inner material). Due to the angle of incoming light being close to $0°$, the light is reflected through the fiber mostly and cannot escape the core. However, with light travelling distances through media, a certain loss of intensity is still inevitable. The amount of light being transmitted through a fiber can be quantified with the beam's intensity at the exit of the fiber [20]:

$$I_{out} = I_{in} \cdot e^{-\alpha \cdot z} \tag{20}$$

$$\alpha = \left(\frac{\mu_{nm}\lambda}{2\pi}\right)^2 \cdot \frac{\nu^2+1}{r_{inner}^3(\nu^2-1)^{\frac{1}{2}}} \qquad \nu = \frac{n_{outer}}{n_{inner}} \tag{21}$$

With $z$ being the axis along which the light propagates, $\nu$ the ratio between the refraction indexes $n_{outer;inner}$ of cladding and core, $r_{inner}$ the radius of the core. $\mu_{nm}$ refers to the m'th root of the Bessel function of the order n, which acts as dimensionless parameter for the $EH_{nm}$-mode.
In figure 4, you can see the transmission rate plotted against the fiber length. As you can see, the longer the fiber, the stronger the higher modes get filtered out. This is why in our experiment, a 3.2 m fiber was used.

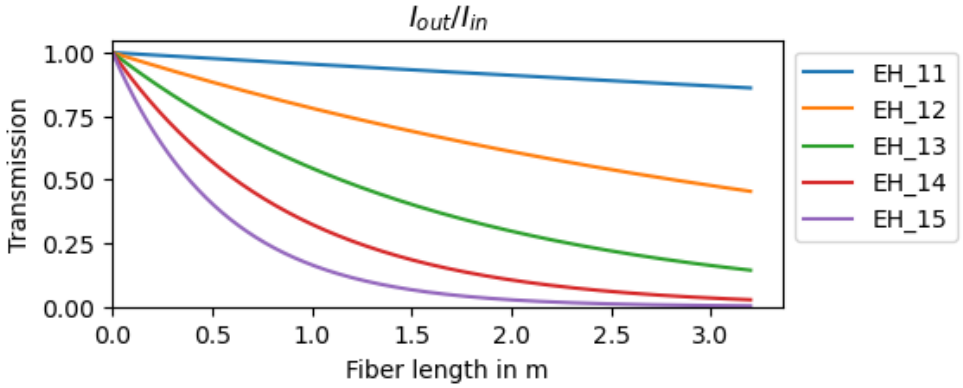


Figure 4: Intensity out/in, mode factors: [1] for a 3.20 m long fiber with $r_{inner}$=265$\mu m$

We can also compute the coupling coefficient $\eta_m$ for a beam with a Gaussian spatial profile in these

modes with[16]:

$$\eta_m = \frac{|\int_0^{r_{inner}} e^{-\frac{r}{w_0}^2} J_0(\frac{EH_{nm}r}{r_{inner}}) r\ dr|^2}{(\int_0^{\infty} e^{-2\frac{r}{w_0}^2} r\ dr) \cdot (\int_0^{r_{inner}} J_0^2(\frac{EH_{nm}}{r_{inner}}) r\ dr)} \tag{22}$$

$r$ is the radial coordinate of the beam, $r_{inner}$ is the fiber core radius and $w$ is the radius of the Gaussian beam waist. Equation 22 results from the overlap integral of a spatial Gaussian beam with a zero-order Bessel function. The coupling coefficient is the physical quantity used to measure how much power goes into each mode.

As you can see in figure 5, the coupling coefficient for the $EH_{1,1}$-mode is significantly higher than for the other modes at roughly $0.6\frac{w_0}{r_{inner}}$ . $w_0$ is the radius of the focused Gaussian beam. In our case this maximum's ratio is optimal , as we want the beam to couple into the $EH_{1,1}$-mode as strongly as possible.

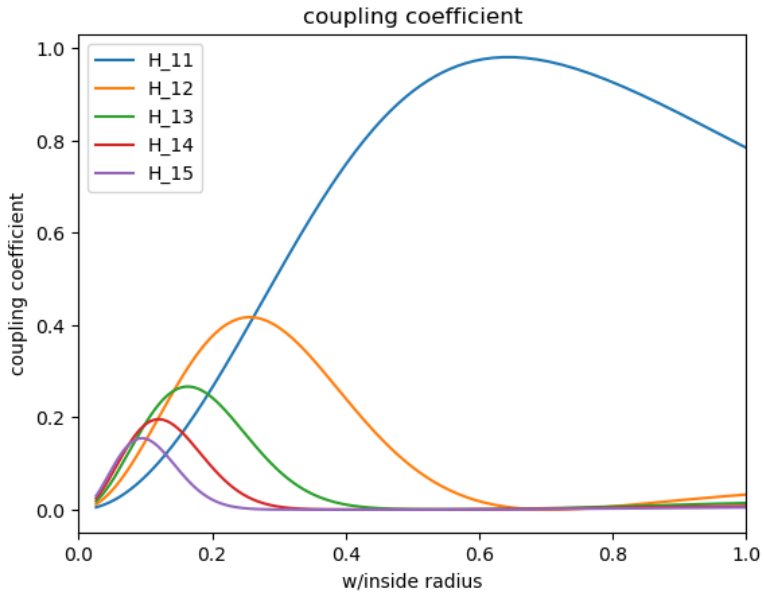


Figure 5: Coupling coefficient against the ratio of beam waist to core radius

The pressure $p(z)$ inside of the hollowcore fiber can simply be derived from fluid dynamics and corresponds to [7]:

$$p(z) = \sqrt{p_1^2 + \frac{z \cdot (p_2^2 - p_1^2)}{L}} \tag{23}$$

with $L$ as the fiber length, $p_1$ as the pressure at the start of the fiber and $p_2$ as the pressure at the end of the fiber. It is important to take the pressure into account, as the light's interaction with the gas is the cause for spectral broadening. Thus, the pressure at each position of the fiber is a crucial quantity. It can also influence the refractive index.

## 4.5 Dispersion

Derived from the Maxwell equations, the behavior of light in media can be expressed with the linear wave equation:

$$\vec{\Delta}^2 \vec{E} - \frac{1}{c^2} \frac{\partial^2 \vec{E}}{\partial t^2} = \mu_0 \frac{\partial^2 \vec{P}}{\partial t^2} \tag{24}$$

with $\vec{E}$ as the electric field of the light, $\mu_0$ as the vacuum permability, $\vec{P}$ as the polarization and $t$ as the time. The main type of dispersion I will be looking at is chromatic dispersion. It can be caused by a change of the refractive index $n$ due to e.g. another medium. Chromatic dispersion can also occur due to the boundary condition at the fiber surface and, by extension, the geometry of the waveguide. The

Polarisation derived from equation 24 is calculated as such:

$$\vec{P}(\vec{r},t)^L = \epsilon_0 \chi^{(1)} \vec{E}(\vec{r},t) \tag{25}$$

$\chi^{(1)}$ is a tensor that shall be explained further in chapter 4.6. For now, it is only relevant to know that the linear susceptibility $\chi^{(1)}$ is a matrix, which for nonmagnetic materials is directly tied to the refractive index through the following relation:

$$n = \sqrt{1 + \chi^{(1)}} \tag{26}$$

The beam's dispersion is affected by the medium's refractive index. This is crucial for the development of the beam's structure through time. With the refractive index, it is possible to describe the dispersion. Thus, the propagation constant $\beta(\omega)$ must be computed. $\beta(\omega)$ is a key parameter to calculate the beam's dispersion and depends of the refractive index $n(\omega)$. It is often also displayed through its taylor polynomial around the central frequency $\omega_0$ of the laser pulse instead:

$$\beta(\omega) = n(\omega)\frac{\omega}{c} = \beta_0 + \beta_1(\omega - \omega_0) + \frac{\beta_2}{2}(\omega - \omega_0)^2 + \frac{\beta_3}{6}(\omega - \omega_0)^3 + ... \tag{27}$$

$$\beta_m = \left(\frac{\partial^m \beta}{\partial \omega^m}\right)_{\omega=\omega_0} \tag{28}$$

The parameter $\beta_0$ affects the phase velocity $v_p$ as such:

$$v_p = \frac{\omega_0}{\beta_0} = \frac{c}{n(\omega_0)} \tag{29}$$

The parameter $\beta_1$ determines the group velocity $v_g$:

$$\beta_1 = \frac{1}{v_g} = \frac{1}{c}\left(n + \omega\frac{\partial n}{\partial \omega}\right) \tag{30}$$

The parameter $\beta_2$ determines the group velocity dispersion (GVD):

$$\beta_2 = \frac{1}{c}\left(2\frac{\partial n}{\partial \omega} + \omega\frac{\partial^2 n}{\partial \omega^2}\right) \tag{31}$$

This is the first and typically dominant parameter of the Taylor expansion that leads to actual dispersion, meaning that the different frequency components of a short pulse will change their relative position in time. Consequently, a bandwidth limited pulse traveling through a medium with dispersion will become longer in time while remaining the same spectral width.
Most materials have a positive GVD, implying so-called *normal dispersion*. However, there are some materials with a negative GVD, leading to *anomalous dispersion*. The dispersion properties are in general frequency and consequently wavelength dependent. Anomalous dispersion for example typically appears when the beam frequency is close to an absorption resonance, but can also be present in transparent media.
An important parameter in this context is the 0- dispersion wavelength $\lambda_D$, which corresponds to the wavelength at which $\beta_2$ becomes 0 (between normal/anomalous dispersion). $\lambda > \lambda_D$ and $\beta_2 < 0$ cause in anomalous dispersion effects in the fiber.
The parameter $\beta_3$ describes the *third order dispersion* (TOD). It only becomes relevant when the second order dispersion effects are close to zero, implying $\lambda \to \lambda_D$. This would happen for instance if a bandwidth limited pulse's central wavelength was close to the 0-dispersion wavelength, or if a combination of different materials summed up to a GVD close to zero.
The group delay dispersion (GDD), which is the wavelength-space equivalent of the GVD, can be ex-

pressed through the parameter $D$:

$$D = \frac{\partial \beta_1}{\partial \lambda} = -\frac{2\pi c}{\lambda^2}\beta_2 \approx \frac{\lambda}{c}\frac{\partial^2 n}{\partial \lambda^2} \tag{32}$$

In this work, it is specifically light propagation through a fiber that is considered and therefore one must not only take the dispersion of spatial propagation through a medium into account, but also the dispersion of the mode propagation constant in the fiber $MPC_{n,m}$ of the $EH_{n,m}$ modes.

$$MPC_{n,m} = \frac{2\pi}{\lambda}\left[\frac{1}{2}\left(\frac{\mu_{n,m}\lambda}{2\pi r_{inner}}\right)\right] \tag{33}$$

This is relevant, as the light propagation speed inside the fiber does not only depend on the wavelength, but also the mode.
The influence of the mode propagation constant on the group velocity, the GVD and the TOD can be deduced analogously to the propagation constant in the equation 27 above.
To estimate the importance of the different dispersion effect it is useful to look at some examples. In figure 6 the inverse group velocity and GVD in several noble gases and for different modes are shown. The wavelength dependent refractive indices were computed using Sellmeier equation [10] and fitting parameters for argon [17], neon [2] and helium [11]. Argon shows the highest normal dispersion followed by neon and helium possesses the lowest GVD. The GVD for the fiber modes is in fact negative and consequently can be minimized inside of the fiber. For example a pulse with a central wavelength of 1.5 $\mu$m coupled into a 3 m long fiber with a 530 $\mu$m diameter will be subject to a GVD of $-37$ fs$^2$ in the $EH_{1,1}$ mode. When filling the fiber with argon to a pressure of 1.28 atmosphere, the gas will lead to a GVD of 37 fs$^2$, showing that the dispersion can be in a similar order of magnitude.
In practice, the beam will usually travel through air and possibly be transmitted through some other medium, resulting in additional, typically normal, dispersion.
Multiple materials exist which are transparent and have a negative GVD in the near infrared spectral range. A selection of them is shown in figure 7. The wavelength dependent refractive indices were taken from different sources [9, 19, 10]. We can see that lower frequencies propagates faster than higher ones in the GV diagramm. As can be observed for a wavelength roughly above 1 $\mu$m, the KDP and ADP crystals have a negative GVD on the ordinary crystal axis, leading to anomalous dispersion. [1] For longer wavelengths, even more materials with this property exist. Interestingly enough all the materials, regardless of whether they cause normal or anomalous dispersion, possess a positive TOD. The TOD is stronger for higher frequencies.
Consequently, the previously accumulated positive GVD can be compensated for using just transmission through proper crystals with a negative GVD. The TOD has to be compensated for by other means, as all materials only possess a positive TOD to the best of my knowledge.

[1] The extraordinary and ordinary crystal axes are terms used to describe anisotropic crystals.

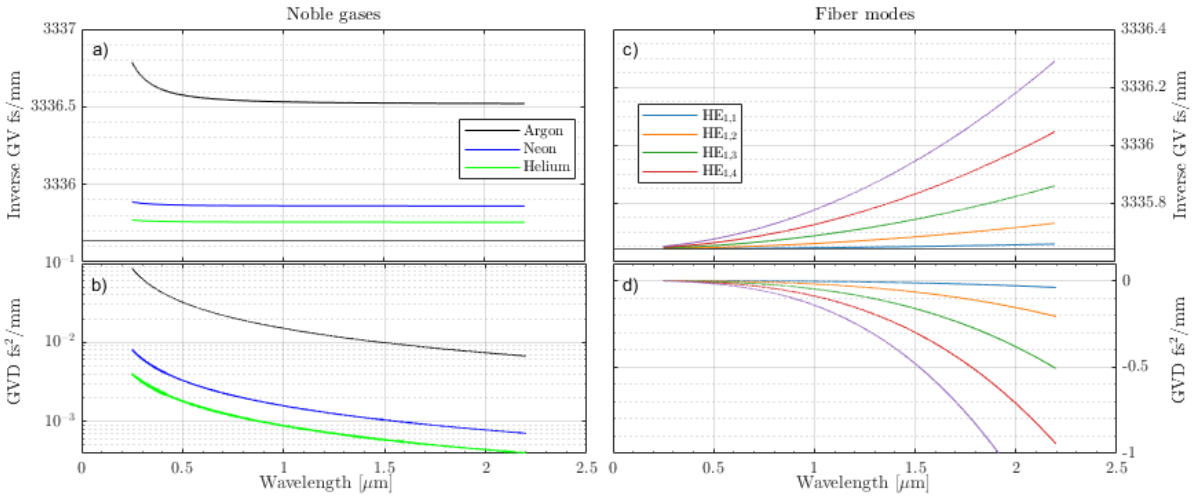


Figure 6: Wavelength dependent a) inverse group velocity and b) GVD of varying noble gases at atmospheric pressure, c) Inverse group velocity for light propagating in different modes of a fiber with 530 $\mu$m diameter,d) GVD for the different modes

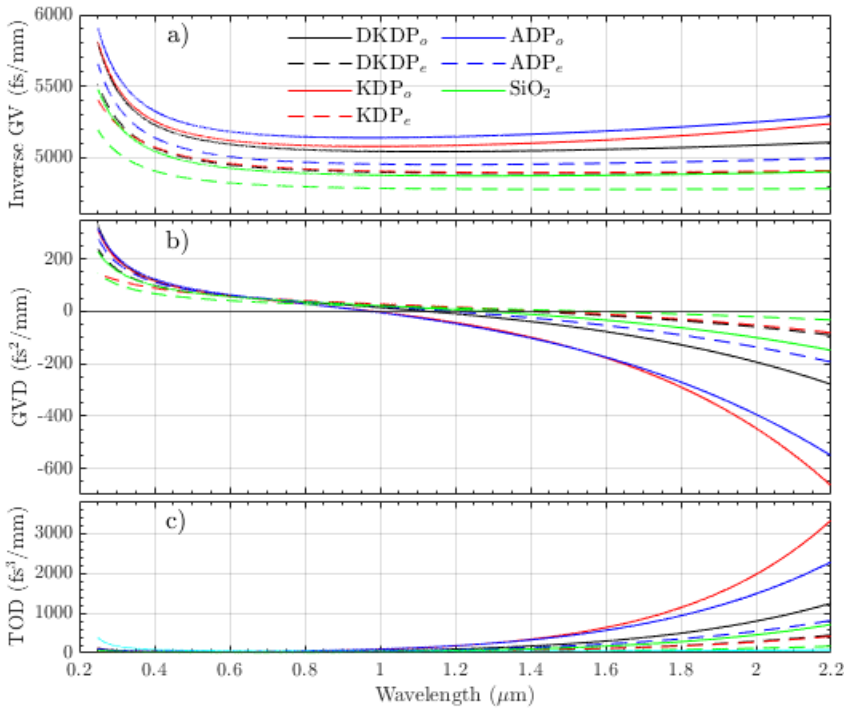


Figure 7: a) Inverse group velocity b) GVD and c) TOD of different materials with anomalous dispersion in the near infrared

## 4.6 Nonlinear medium response

Typically, the polarization response induced by an electric field in matter grows proportionally to the field strength. If the field strength reaches a magnitude that is around 0.1% of the the atomic field or more, the electron displacement will no longer change proportionally to the electric field. In this case, understanding *nonlinear optics* is crucial. First, pertubation theory can be used to describe the induced

nonlinear polarization $P$:

$$\vec{P}(\vec{r},t) = \underbrace{\epsilon_0\chi^{(1)}\vec{E}(\vec{r},t)}_{P^L} + \underbrace{\epsilon_0\left(\chi^{(2)}E\vec{E}(\vec{r},t) + \chi^{(3)}E\vec{E}E(\vec{r},t) + ...\right)}_{P^{NL}} \tag{34}$$

Here, the susceptibility $\chi^{(n)}$ is a tensor of the rank $n+1$. For instance, $\chi^{(1)}$ is a matrix that describes linear optics. The different $\chi^{(n)}$ are responsible for different effects. For example, $\chi^{(1)}$ determines the double refraction, where one light beam is split up in two orthogonally polarized beams upon entering certain media. [2]

To put it simply, the susceptibility determines how an electric field reacts to a certain medium. In an isotropic (meaning independent of spatial orientation), homogenous medium and in case of the absence of nonlinear effects, this can be expressed with the formula:

$$\vec{P} = \chi\epsilon_0\vec{E} \tag{35}$$

This becomes more complicated when the aforementioned conditions are not guaranteed and the equation 34 must be used.

Usually, using only the first (linear) term is sufficient to approximate $\vec{P}$. However, when dealing with very intense light, the electric field becomes so strong that higher (nonlinear) orders need to be taken into account. Basically, the term *linear optics* means the limit for the weak field, in which only the first order of susceptibility $\chi^{(1)}$ needs to be considered.

To calculate the exact nonlinear part of the nonzero nonlinear polarization $\vec{P}^{NL}$, the nonlinear wave equation

$$\left(\nabla^2 - \left(\frac{n}{c}\right)^2\frac{\partial^2}{\partial t^2}\right)\vec{E}(\vec{r},t) = \mu_0\frac{\partial^2}{\partial t^2}\vec{P}^{NL}(\vec{r},t) \tag{36}$$

needs to be considered. The left handside contains the linear wave equation, whilst the right handside contains the nonlinear polarization term. The latter is responsible for driving new fields if it oscillates at a different frequency than the driving field. If the polarization's frequency does match the driving field's frequency, the newly generated fields can interact with the driving field.

In the following, I will take a closer look at the most dominant effects that may perturb the field by analyzing the lowest nonlinear polarization orders. Firstly, even orders of the susceptibility $\chi^{(n)}$ only contribute in non-isometric crystals, as they are otherwise parity-forbidden and noble gases for instance only have odd orders of susceptibility. Now, let's consider the non-isometric crystal case.

Let's have a closer look at the second term of equation 34:

$$\chi^{(2)}\vec{E}\vec{E}(\vec{r},t) = \chi^{(2)}\left[E_0\cdot e^{-i(\omega_0 t-\vec{k}\cdot\vec{r})} + c.c.\right]^2 = \chi^{(2)}\left(2|E_0|^2 + E_0^2e^{-2i(\omega_0 t-\vec{k}\cdot\vec{r})} + E_0^{*2}e^{2i(\omega_0 t-\vec{k}\cdot\vec{r})}\right) \tag{37}$$

The first term $2|E_0|^2$ is responsible for light inducing a direct current field in its medium. This effect is called optical rectification (OR). The other two terms are responsible for generating the second harmonic light with the frequency $2\omega$ (second harmonic generation SHG). In order to maximize the SHG output, the light inside the medium must be coherent.

Now let's have a look at how this would work with a combination of two different electric fields $E_1$ and $E_2$:

$$\tilde{\vec{E}}(t) = \vec{E_1}e^{-i\omega_1 t} + \vec{E_2}e^{-i\omega_2 t} + c.c. \tag{38}$$

$$\tilde{\vec{P}}^{(2)}(t) = \epsilon_0\chi^{(2)}\tilde{\vec{E}}(t)^2 \tag{39}$$

[2] This effect will not be important in this work though. Other more relevant effects, like the Kerr effect, which is determined by $\chi^{(3)}$ will be further discussed in the next section.

This adds many additional terms to $\tilde{\vec{P}}$ [3]:

$$\begin{aligned}
\vec{P}(2\omega_1) &= \epsilon_0\chi^{(2)}\vec{E_1}^2 && (SHG) \\
\vec{P}(2\omega_2) &= \epsilon_0\chi^{(2)}\vec{E_2}^2 && (SHG) \\
\vec{P}(\omega_1+\omega_2) &= 2\epsilon_0\chi^{(2)}\vec{E_1}\vec{E_2} && (SFG) \\
\vec{P}(\omega_1-\omega_2) &= 2\epsilon_0\chi^{(2)}\vec{E_1}\vec{E_2}^* && (DFG) \\
\vec{P}(0) &= 2\epsilon_0\chi^{(2)}\left(\vec{E_1}\vec{E_1}^* + \vec{E_2}\vec{E_2}^*\right) && (OR)
\end{aligned} \tag{40}$$

Consequently, a field at new frequencies are generated. Additonally, the individual *second harmonic generation* (SHG) of the drivers, the combined *sum frequency generation* (SFG) and the *different frequency generation* (DFG) appear. The latter is the only process that enables the generation of lower frequencies and will be used in this work to generate a wavelength that is closer to the near-IR than the driving laser. Thus, using two different electric fields is necessary in order to tune whatever wavelength is desired, which is obtained by substracting $\omega_2$ from $\omega_1$.

Let's consider the third-order of the polarization equation 34. Assuming only one frequency of the driving field (as the third order would otherwise become very complicated). The third order polarization results in term of the same frequency as the fundamental and third harmonic generation[3]:

$$\vec{P}(3\omega) = \chi^{(3)}\vec{E_0}^3 \tag{41}$$

$$\vec{P}(\omega) = 3\chi^{(3)}\vec{E_0}\cdot\vec{E_0}^*\vec{E_0} \tag{42}$$

The nonlinear component will be rewritten as follows in this section:

$$\bar{n_2} = n_2 * 2\epsilon_0 cn \approx n_2 * 2\epsilon_0 cn_0 \tag{43}$$

Assuming a field that can be described with $\tilde{E}(t) = E(\omega)e^{-i\omega t} + c.c.$, the refractive index can be put in relation to the linear refractive index $n_0$ and the nonlinear component $n_2$:

$$n = n_0 + 2\bar{n}_2\left|E(\omega)\right|^2 \tag{44}$$

This change of refractive index is, as I shall later discuss, called the *Kerr effect*.
The effective susceptiptibility $\chi_{eff}$ is a variable that is useful to summarize the effect of $\chi^{(1)}$ and $\chi^{(3)}$ on the refractive index. It is expressed as such:

$$\chi_{eff} = \chi^{(1)} + 3\chi^{(3)}\left|E(\omega)\right|^2 \tag{45}$$

and can be inserted into the following relation:

$$n^2 = 1 + \chi_{eff} \tag{46}$$

Combining the equations 44 and 46 yields:

$$\left[n_0 + 2\bar{n_2}\left|E(\omega)\right|^2\right]^2 = n^2 = 1 + \chi^{(1)} + 3\chi^{(3)}\left|E(\omega)\right|^2 \tag{47}$$

This shows the relation between the linear and nonlinear refractive indices to the linear and nonlinear

susceptibilities [3], which can be described as:

$$n_0 = \left(1 + \chi^{(1)}\right)^{\frac{1}{2}} \tag{48}$$

$$\bar{n_2} = \frac{3\chi^{(3)}}{4n_0} \tag{49}$$

This underlines again how $\chi^{(1)}$ is specifically responsible for the linear refractive index and $\chi^{(3)}$ for its shift. This brings me to the next section, where I shall look more closely at this shift and the other effects it causes.

### 4.6.1 Self-phase modulation, self-steepening and self-focusing,

*Self-phase modulation* (SPM) is a nonlinear optical effect that can be observed on ultrashort pulses. It is caused by the *Kerr-effect*, where light induces an electric field which affects the refractive index as follows:

$$n(I) = n_0 + n_2 \cdot I \tag{50}$$

Consequently, the refractive index is higher where the beam is more intense. Coincidentally, this also causes the beam to focus itself (*self-focusing*). In figure 8, a visualisation of how self-focusing occurs is shown. The less intense edges of the Gaussian beam are subject to a lower refractive index and are thus redirected more strongly towards the center. This is similar to the way convex lenses work.

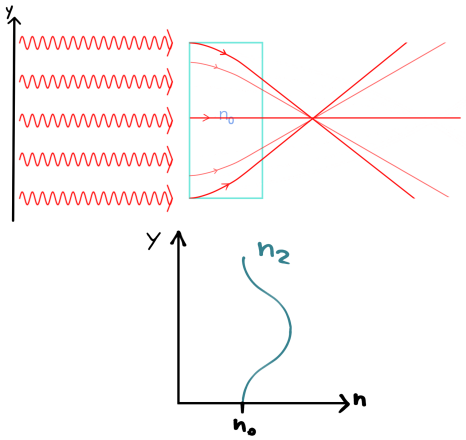


Figure 8: Self-focusing with arbitrary units for the spatial component $y$

Another change caused by the Kerr-effect is the *self-steepening* of the pulse. Due to the increased refractive index $n(I)$, the light propagates more slowly depending on the intensity through the medium. This causes a shift of the intensity distribution of the pulse $I(t)$, and the start of the pulse becomes more intense, while its end becomes longer.
An example of a self-steepened pulse is provided in figure 9. You can observe you the self-steepened pulse falls off much quicker than it rises and thus becomes asymmetric. The spectrum is also modified. The higher frequency spectrum is broadened and becomes less intense, while the lower frequency spectrum becomes more intense. [3]

[3]The nonsense part is due to the fact that this physical model becomes inaccurate in case of a too strong self-steepening effect. The spectrum appears to be infinitely broadened as the right slope of the pulse becomes perpendicular to the time-axis.

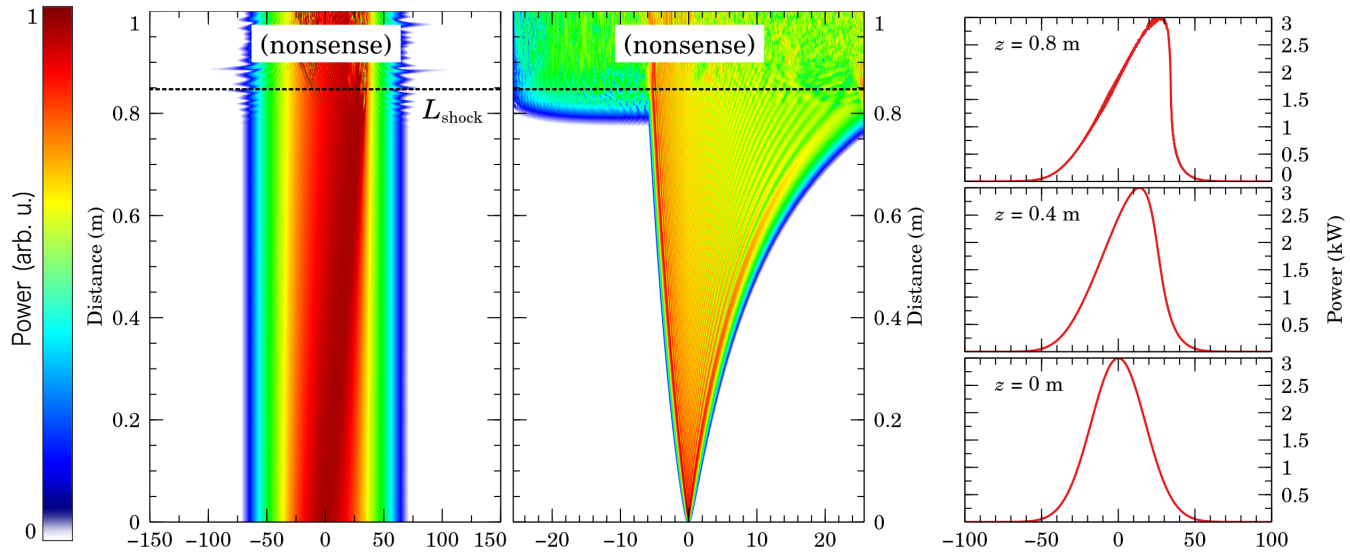


Figure 9: Self-steepening of an arbitrary pulse in a fiber, power against time and distance, power against frequency and distance [14]

The alteration of $n$ also causes a phase shift in the spectrum:

$$\Delta\Phi_{NL}(t) = \frac{\omega_0 n_2}{c} \cdot L\ I(t) \tag{51}$$

which alters the frequency spectrum:

$$\omega(t) = \omega_0 - \frac{\Delta\Phi_{NL}(t)}{dt} \tag{52}$$

This produces different symmetric frequency shifts for different areas (in time) of the pulse. This frequency shift is named self-phase modulation. Figure 10 shows a self-phase modulated pulse at different locations in a fiber. As we can see, the spectrum becomes increasingly broader. The intensity peaks at the spectrum's borders.

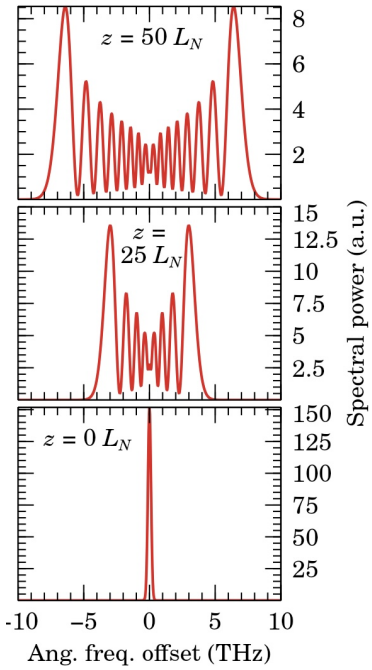


Figure 10: SPM of an arbitrary pulse having travelled different distances $L_n$ in a fiber [13]

### 4.6.2 Ionization

The laser pulses inside of the hollowcore fiber can ionize atoms of the gaseous medium inside the hollowcore fiber creating a plasma. This can occur through various processes. Electrons can, for instance, be detached from their atoms if they interact with a photon of the beam that has a sufficiently high frequency. However, ionization through light is still possible even if the beam's frequency is inferior to the atom's binding energy for the latter phenomenon. As our short laser pulses are very intense, it is possible for the atom to absorb several photons at once which's combined energies can overcome the atom's ionization energy. This is called Multiphoton Ionization (MPI). If the laser beam is even more intense, its electrical field can distort the atoms' potential, possibly causing electrons to tunnel out of it.
The Keldish parameter $\gamma_K$ serves as a means to determine which process dominates. If $\gamma_K \gg 1$, MPI will be the more relevant effect, while $\gamma_K \ll 1$ indicates that potential distortion will dominate. This parameter can be calculated as follows:

$$\gamma_K = \frac{\omega_0}{eE_{laser}} \sqrt{2m_e U_I} \tag{53}$$

with $U_I$ as the ionization potential, $E_{laser}$ as the peak electric field, $\omega_0$ as the central frequency $m_e$ as the electron mass $9.1093837015 \cdot 10^{-31}$ kg and $e$ as the elementary charge $1.602176634 \cdot 10^{-19}$ C.
Having free electrons inside the waveguide is problematic, as it influences the refractive index. The refractive index of the plasma succumbs the change $n_p$:

$$\Delta n_p \approx \frac{-\omega_p^2}{2\omega_0^2} \tag{54}$$

$$\omega_p = \sqrt{\frac{e^2 \rho_e}{m_e \epsilon_0}}$$

Here, $\omega_p$ is the plasma frequency. As the electrons in the plasma are being attracted by the ions, they can oscillate around the latter. The frequency at which they oscillate results in the plasma frequency. This plasma frequency causes a blue-shift in the spectrum of the light beam. $\rho_e$ designates the free electron

density. If a medium is subject to ionization through MPI and tunnel-ionization, the free electron density will first increase exponentially with time and then deaccelarate slowly until it reaches a plateau. The scale of this effect greatly depends on the beam's peak intensity. Ideally, $\Delta n_p$ should be minimal. In our case, the setup ensures that is the case. The effect is irrelevant compared to the Kerr effect. For example, the gas inside the fiber is a noble gas, greatly reducing the risk of possible reactions and ionizations. Still, the refractive index shift is taken into account in the simulation.

# 5 Experimental setup

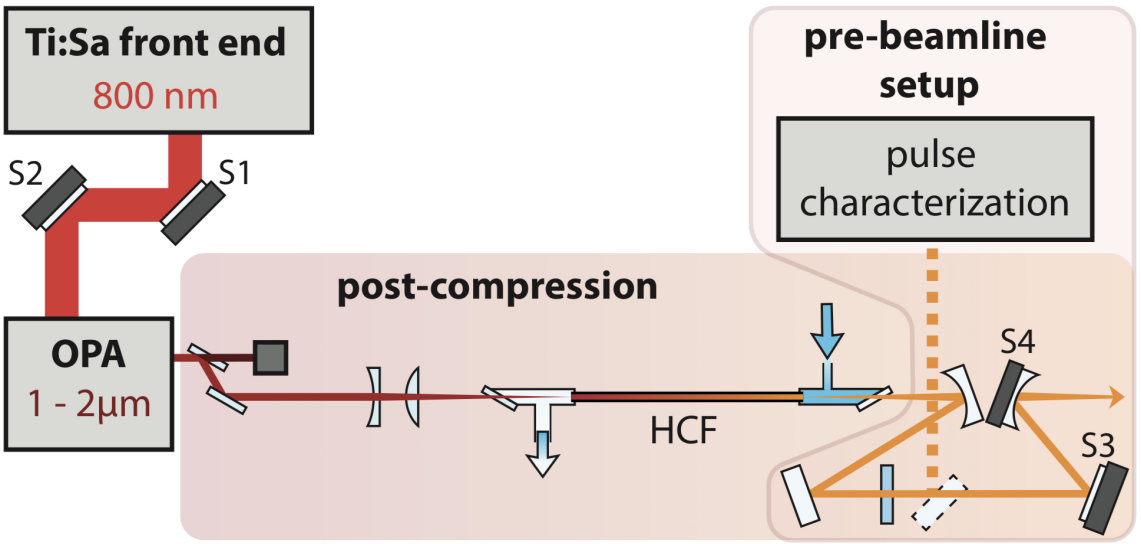


Figure 11: Schematic overview of the experimental setup with the Ti:Sa, the OPA and the hollowcore fiber (HCF) [21]

In this chapter, I will describe the setup of the experiment which provided me with data to compare to my simulation. I will also explain how chirped pulse amplification and parametric down conversion works. The setup uses a Ti:Sa laser to generate short pulses centered at 800 nm, which are used to seed an optical parametric amplifier (OPA). The signal produced by the OPA is then focused using a lens telescope into the hollowcore fiber, which can be filled with a noble gas allowing for spectral broadening.

## 5.1 Overview

In our case, we want a device capable of emitting ultrashort pulsed laser beams. In order to achieve such a short pulse duration of the magnitude of femtoseconds, the beam must be extremely powerful as we need to make use of the nonlinear effects in order to sufficiently broaden the spectrum.
A schematic overview of the experimental setup is provided in figure 11. The master laser of the experimental setup is a Ti:Sa (titanium-doped-saphire) laser, which makes use of the principle of chirped pulse amplification to generate intense (up to 22 mJ), short ($\approx$ 30 fs) pulses with a 1 kHz repitition rate. A short description of the laser will be given later on in this chapter. The Ti:Sa laser generates light with a broad spectrum around the central wavelength at 800 nm. In order to permit better tuning and allow for being more flexible with the output wavelength in the near infrared, an *optical parametric amplifier* (OPA) is seeded with the Ti:Sa laser pulses. Using the principle of *parametric down conversion*, light pulses with a central wavelength within the boundary of $1.1\mu m < \lambda < 2.4\mu m$ can be generated. These pulses are then sent into the hollowcore fiber for *pulse broadening*, which is the main subject of this thesis. The hollowcore fiber serves as post-compression device, making use of the nonlinear self-phase modulation process. It was chosen to be hollow and filled with gas, as it is easier to avoid permanent damage with this media and as certain parameters, like e.g. pressure, can be changed and managed more easily. Having a gas-filled fiber, however, means the core (with most gases) has a smaller refractive index than the cladding. This might present some difficulties to keep the light inside the fiber. The transmission rate could be increased by widening the core radius as can be deduced from equation 21 , but this would also decrease the peak intensity.

When focusing a beam, the focus width is proportional to the focus length. This means focusing over long distances leads to a relatively wide beam at the focal point. So in order to couple the beam well into the fiber, which is relatively long, a larger fiber diameter ($2r_{inner}$) is preferable. The a wider fiber diameter also means there will be less intensity losses caused by absorption, as these losses scale with $\sim r_{inner}^{-3}$.
The beam needs to to propagate over a long distance through the gas inside the fiber to increase the spectral broadening enough. Hollowcore fibers bear the advantage compared to other methods that its length has practically no upper limit, and that it can be applied to different wavelengths without changing the whole setup.

In order for the beam to couple into the hollowcore fiber efficiently, it must be well characterised. Losses in the fiber are mainly due to the mode coupling, as well as a dampening along the beam's trajectory. The magnitude of the pulse's power is in the milijoules.

## 5.2 Laser

Lasers are a type of light source and are distinguished by their strong coherence. Other light sources usually emit photons in randomly timed relatively incoherent bunches. By contrast, lasers emit their pulses of photons in a timed and coherent manner. There are also "cw lasers", which continiously emit photons, but they are irrelevant for this work. Laser beams can propagate over long distances while maintaining their high intensity due to their low divergence and great coherence length, the latter meaning the photons have an approximately constant phase to each other. They also typically differentiate themselves from other light sources by the high peaks they can achieve, as well as the narrowness of their cross-section (meaning the area of the beam waist).
Essentially, a laser system can be constructed with two mirrors forming a cavity, a gain medium in between the mirrors and a pump source. The pump source sends light or electrons to the gain medium in order to provoke a population inversion, meaning that it will cause more atoms to move to a higher energy state. This, in turn, can lead to stimulated and spontaneous emission. The gain medium is enclosed by 2 parallel mirrors, one of which is highly reflective and the other one being partially reflective. Thus, the emitted photons which propagate vertically to the mirrors can be reflected back into the medium to stimulate more emission. The new emitted photons have the same wavelength and move in the same direction as those which stimulated them. This process of stimulated emission and of the photons staying between the two mirrors causes a chain reaction, which increases the number of photons exponentially. As one of the two mirrors is merely partially reflective, some of the photons can exit this resonating chamber. These photons constitute the laser beam.

## 5.3 Chirped pulse amplification

Chirped pulse amplification is used specifically here to amplify the light beam that enters the TOPAS.
In general, this method is used for lasers desired to have a high pulse energy and a short pulse duration. Since every crystal has a damage threshhold, corresponding to a certain peak power or peak power per area, this is particularly challenging for short pulses which reach high peak powers. Thus, we use chirped pulse amplification to avoid material damage and still achieve high pulse energies.
First, the output of an oscillator with $\sim 10^1$ fs pulse durations is strongly chirped, stretching the pulse to tens or hundreds of picoseconds, meaning that that the pulse's individual frequencies are being delayed from each other. With the peak intensity reduced by orders of magnitude, the pulses are amplified in a gain medium, usually crystal. This process can be done multiple times using an amplification chain reaching pulse energies that are magnitudes higher at the output compared to the input pulses. Finally,

the amplified pulse is compressed again, thus reverted to it's original duration.
First adding and then removing a chirp bears the advantage that the amplified beam will not damage the optics as much, as the frequencies do not arrive at the same time, but are delayed.
Chirping and compressing the pulses is usually done with stretchers and compressors using dispersive grating, leading to a different beam path length in these devices.

## 5.4 Optical parametric amplifier

The TOPAS (*Light Conversion TOPAS HE Prime+*) is an optical parametric amplifier. It's purpose is to use the incoming light beam to obtain a pulse of a specific wavelength. An optical parametric amplifier is a type of amplifier making use of parametric down conversion instead of stimulated light emission. Consequently, it needs a seeding beam. The HE-TOPAS used for this work is seeded with 18 $mJ$ pulses from the aforementioned Ti:Sa laser. A sketch of the working principle of the TOPAS is provided in 12. A major part of the pump beam (98%) is first reflected and then used as a pump in the last stage. The remaining 2% are transmitted and used to generate the seed signal for the last stage. A part of the beam is focused onto a glas plate for signal generation. This leads to white light generation (WLG).
This light finally meets up with a weak pump beam inside a nonlinear BBO crystal. This is where parametric down conversion occurs and a certain spectral range of the seeding white light is amplified. Before entering the crystal, the white light is despersed (stretched). Therefore, the time delay can be tuned, allowing to generate a signal beam featuring a central wavelength between $\sim 1.1\mu m - 1.5\mu m$ . This signal beam is then used to seed a second crystal pumped by another fraction of the 800 nm beam. Finally, the now amplified signal beam ($\approx$ 100 $\mu$J) is used to seed the last BBO crystal, converting up to 40% of the pump's energy into the idler and signal beam. In this work, the idler beam and the pulse energy are estimated at about 1440 nm and 4 mJ and an estimated pulse duration of 40 fs has been used.

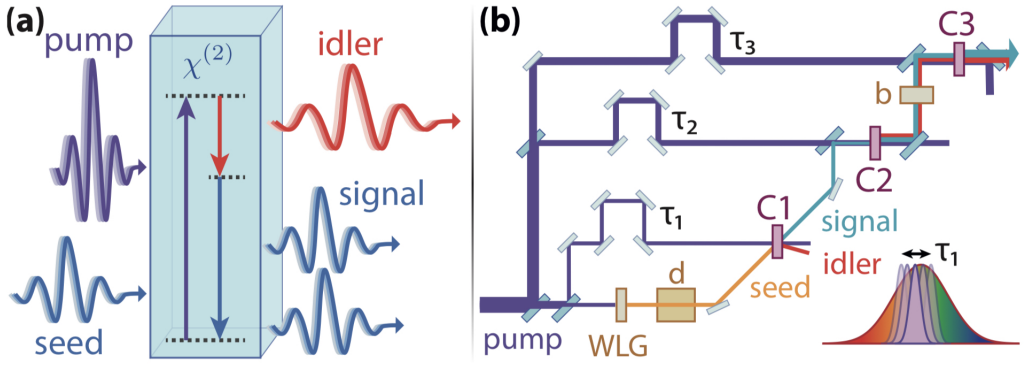


Figure 12: Optical parametric amplification
from [21]

### 5.4.1 Signal and idler

The pump photon (here $E_{pump} = 1.55eV$) is converted into two less energetic wavelengths by means of absorption and emission. One of these emitted photons is the signal and the other one is called idler (see figure 12*(a)*). The signal and idler are called parametric output photons. Their energy must be conserved:

$$\omega_{pump} = \omega_{signal} + \omega_{idler} \tag{55}$$

### 5.4.2 Tuning the wavelength

Alongside with the pump photon, a *seed* photon is also sent in. It has the same frequency as the signal and serves to stimulate the emission at the intended wavelength. This seed photon is picked out of a white light beam where each frequency arrives at a different time by creating a delay between the pump beam at the first pump branch and it (see figure 12b)). Thus, the wavelength of the resulting signal can be tuned.

## 5.5 The hollowcore fiber

A hollowcore fiber was used in this work in order to broaden the signal pulses from the TOPAS. The fiber is 3.2 m long and has an inner core diameter of 530 $\mu$m. The fiber is glued into two holders, which are then fixed on a manipulator including micrometer tables in order to stretch it out. This contraption allows the precise adjustment of the fiber ends' horizontal and vertical position for in- and out coupling. Both holders include a CF-40 flange and are each connected to a ˜2 m long vacuum chamber. The signal beam of the TOPAS is coupled to the fiber using a lens telescope consisting of a defocusing and a focusing lens placed on an optical slide.
The telescope's purpose is to focus the beam exactly at the entrance of the fiber. This is crucial, as the beam should propagate as evenly as possible through the fiber. Assuming a Gaussian beam, the focus is where the light would propagate as a plane wave.
Using two lenses on a an optical rail allows to focus at the same position with slightly different different focal waists. This is important as it can be seen from equation 22 that coupling into the $EH_{1,1}$ -mode efficiently is only possible with the correct focal size.
In order to further broaden the pulses, the vacuum chamber on the backside of the hollowcore fiber is filled with a noble gas, for instance argon or neon. This results in the pressure inside the fiber being differential. The highest pressure is at the end and the entrance pressure comes close to zero (see figure23).

## 5.6 Parameters

Most of the parameters used were taken from Dr. Rupprecht's Phd thesis [21], as they in part still match those of the current laser system.

| symbol | parameter | value |
|---|---|---|
| $\lambda_0$ | central wavelength | 1.43 $\mu m$ |
| $L$ | fiber length | 3.2 $m$ |
| $r_{inner}$ | radius of fiber core | 265 $\mu m$ |
| $\tau_{FWHM}$ | pulse duration | 40 fs |

# 6 Numerical methods

## 6.1 Nonlinear Schrödinger equation

The propagation of optical pulses through dispersive, nonlinear media can be described as:

$$\frac{\partial A(\tau,z)}{\partial z} = i\gamma|A(\tau,z)|^2 A(\tau,z) - \frac{1}{2}\beta_2 \frac{\partial^2 A(\tau,z)}{\partial \tau^2} \tag{56}$$

The first term on the right-hand side causes the pulses to spread due to SPM and the second one shows how they spread because of the GVD. $\tau$ is the retarded time and corresponds to

$$\tau = t - \frac{z}{v_g} \tag{57}$$

This equation is referred to as the *nonlinear Schrödinger equation* (NSE). It is derived from $E(z,t)$ equation 9, put into a wave equation. The wave equation is written in terms of $A(z,\tau)$ using the complex amplitude , which then results into equation 56 through many transformations.

## 6.2 Generalized nonlinear Schrödinger equation

Assuming Gaussian input signals, one can combine effects such as attenuation $\alpha$, dispersion $\beta$ and nonlinearity $\gamma$ into a slowly varying envelope amplitude $A(z,t)$, Fourier transform this and simplify it into a differential equation:

$$\frac{\partial A(\tau,z)}{\partial z} = \underbrace{-\frac{\alpha}{2}A(\tau,z)}_{\text{absorption}} \underbrace{-\frac{i}{2}\beta_2(z)\frac{\partial^2 A(\tau,z)}{\partial \tau^2}}_{\text{GVD}} + \underbrace{\frac{1}{6}\beta_3(z)\frac{\partial^3 A(\tau,z)}{\partial \tau^3}}_{\text{TOD}} \underbrace{-i\gamma|A(\tau,z)|^2 A(\tau,z)}_{\text{SPM}} \underbrace{-\frac{\gamma}{\omega_0}\frac{\partial}{\partial \tau}\left(|A(z,\tau)|^2 A(z,\tau)\right)}_{\text{self-steepening}} \tag{58}$$

The first term takes the absorption into account. For this, the Beer-Lambert law is assumed. The second and third one are for the GVD and TOD (third order dispersion) respectively, using the already discussed parameter $\beta$ in chapter 4.5. The fourth one is responsible for the SPM and the last one for self-steepening effect. These last two terms result from nonlinear effects. They contain the nonlinearity parameter $\gamma$:

$$\gamma = \frac{\omega_0 n_2}{c A_{eff}} \tag{59}$$

with $A_{eff}$ as the effective mode area which approximately corresponds to $0.48 \cdot \pi r_{inner}$. The slowly varying envelope approximation is only accurate if the pulses are longer than around 10 fs, as otherwise the spectral width would overlap with the carrier frequency.
This formula still has restrictions. By deducing the *generalized nonlinear Schrödinger equation* (GNLSE), several approximations are used, giving limits for parameters at which the equation still describes real light pulses well. For example, using an effective mode area implies that all spatial components of the electric field are modulated with the same strength of nonlinear effects. This approximation becomes particularly problematic when modeling non focused fields, where for example Kerr focusing can be a dominant effect. Secondly, the slowly varying envelope approximation is used for deducing the GNLSE, assuming that the change in time of the envelope is negligible compared to the change of the fast oscillating carrier. Consequently the model becomes worse when the envelope becomes too short and is only a few optical cycles long. It also only considers the direction in which the beam is propagating. The interactions between the $EH_{11}$ mode and higher modes is not taken into account, as they should be strongly repressed anyway. The plasma blueshift is also ignored due to the low density of free electrons.

### 6.3 Split-step Fourier method

In order to approximate the beam's propagation, the program I used operates via the Split-step Fourier Method (SSFM). The differential equation used to compute the slowly varying envelope $A(z,t)$ is:

$$\begin{aligned}\frac{\partial A(\tau,z)}{\partial z} &= (\hat{D}+\hat{N})A(\tau,z) \\ \hat{D} &= i\frac{\beta_2}{2}\omega^2 - i\frac{\beta_3}{6}\omega^3 - \frac{\alpha}{2} \\ \hat{N} &= i\gamma\left|A(\tau,z)\right|^2 - \frac{\gamma}{\omega_0 A(\tau,z)} IFFT\left[i\omega FFT\left(\left|A(\tau,z)\right|^2 A(\tau,z)\right)\right]\end{aligned} \tag{60}$$

$\hat{D}$ and $\hat{N}$ are operators. $\hat{D}$ is the operator for dispersion and $\hat{N}$ is the operator for nonlinear effects. They can almost be directly obtained from the GNLSE 58. The evaluation of the time derivative is executed in the Fourier space, and thus the operators $\frac{\partial}{\partial\tau}$ were replaced with $i\omega$. [8] The dispersion along the $z$-axis is progressively simulated with the step size $h$ from start to end of the fiber. The formula to compute the amplitude at the next $z$ is:

$$A(z+h,\tau) = e^{h\hat{D}}e^{h\hat{N}}A(z,\tau) \tag{61}$$

We start at $z_0 = 0$. This process is separated into two sub-steps. First, $\hat{D}$ is assumed to be dominan $\hat{N} \to 0$ , then the other way around. In order to increase the approximation's accuracy, one can use the symmetrised SSFM. For this, the dispersion term is split up into two $e^{\frac{h}{2}\hat{D}}$ 's and the nonlinear term is put in between them. This yields:

$$A(z+h,\tau) = e^{\frac{h}{2}\hat{D}}e^{h\hat{N}}e^{\frac{h}{2}\hat{D}}A(z,\tau) \tag{62}$$

Using the Baker-Campbell formula, the error in each step of equation 62 is found out to scale with $O(h^3)$, while the result itself scales with $O(h)$, meaning that the relative error scales with $O(h^2)$:

$$\begin{aligned}A^{DN}(z+h,\tau) &= e^{h\hat{D}+h\hat{N}+\frac{h^2}{2}[\hat{D},\hat{N}]+\frac{h^3}{12}[\hat{D}-\hat{N},[\hat{D},\hat{N}]]+\cdots}A(z,\tau) \\ A^{DN}(z+h,\tau) &= e^{h\hat{D}+h\hat{N}-\frac{h^2}{2}[\hat{D},\hat{N}]+\frac{h^3}{12}[\hat{D}-\hat{N},[\hat{D},\hat{N}]]+\cdots}A(z,\tau)\end{aligned} \tag{63}$$

The resulting computation process of the computer to solve equation 62 for each step is:

$$\begin{aligned}A &= A(z,\tau) \\ A' &= IFFT\left(e^{i\frac{\bar{h}}{2}\hat{D}}FFT(A)\right) \\ A'' &= e^{i\bar{h}\hat{N}}A' \\ A''' &= IFFT\left(e^{i\frac{\bar{h}}{2}\hat{D}}FFT(A'')\right) = A(\tau,z+h)\end{aligned} \tag{64}$$

The Fourier transform of $A$ is used, because discrete Fourier transforms can be calculated very quickly by computers. This is often used to make algorithms for simulations more efficient. The Fourier transform allows to simplify the time derivative $\frac{\partial}{\partial\tau}$ to $-i\omega$, which was used to derive the operators in equation 60.

### 6.4 Numerical implementation

My initial task was to solve:

$$i\frac{\partial^2 V}{\partial(z/z_0)} = \frac{\pi}{4}\left[\frac{\partial^2 V}{\partial(t/t_0)^2} + 2|V|^2 V\right] \tag{65}$$

This nonlinear Schrödinger equation is supposed to describe the propagation of a pulse through a fiber with the electric field's potential $V$. It's equivalent to equation 56. I first decided to try to adapt this code[12], which uses the split-step Fourier method. Unfortunately, it turned out it was not as close to my

needs as I first anticipated and I did not succeed in getting it running properly with all of the parameters that need to be kept in mind for our hollowcore fiber.
Next, I had a look at a code belonging to the group of Jan-Hendrik Oelmann meant for computing the propagation of a pulse through a multi-pass cell. I realized this was even further from what I needed to simulate light in a hollowcore fiber than the previous code due to the different geometrical setup, so this idea was quickly discarded.
I also discarded this Schrödinger equation 65, as it only takes self-phase modulation into account. The self steepening effect is not taken into consideration and thus the equation is not suited for pulses shorter than $ps$-pulses. As we are using $fs$-pulses, a more complete equation 58 was going to be required.
Finally, my attention was brought on to the program Luna[4], which is useful for the simulation optical nonlinear processes and is also highly adaptable to very specific setups and geometries if needed so. This is the program I ended up building upon to obtain the data showcased in this thesis.

# 7 Results

## 7.1 Computing with Julia

The program I mainly used to compute my numerical results was Luna[4], which is written in Julia. Julia is a programming language rooted in C, C$^{++}$ and Scheme, which is well suited for running numerical simulations due to its high efficiency. Thanks to this, running my beam propagation simulation only takes a couple of seconds.
Luna is a program used for the simulation of nonlinear optical dynamics in waveguides and in free-space geometry. In my case, I aim to simulate a laser-beam inside a waveguide, namely a hollowcore fiber. For this, Luna should operate with the generalized nonlinear Schrödinger equation 58.
In order to extract the desired data, I used my custom code which employed Luna functions. The set parameters correspond to those of the real fiber.
The used solving mechanism was the split-step-method, which was directly applied by Luna.
Solving the GNLSE can be achieved by setting up Luna using only the Kerr effect as nonlinear response and setting the full field calculation to false. Thus Luna is restricted to calculate only with the envelope. Additionally the fiber parameters needs to be inserted, with a diameter of 530 $\mu m$ and propagation in the $EH_{1,1}$ mode in this first example. The gradient pressure is based on equation 23 can be directly implemented, too. For a given target gas, in this case neon, the increasing nonlinearity parameter $\gamma$ along the fiber is computed by Luna.
Last but not least a proper input pulse needs to be set. In the first example we used a pulse energy of 3 mJ, a 1430 nm central wavelength and a pulse duration of 50 fs for a Gaussian temporal profile.

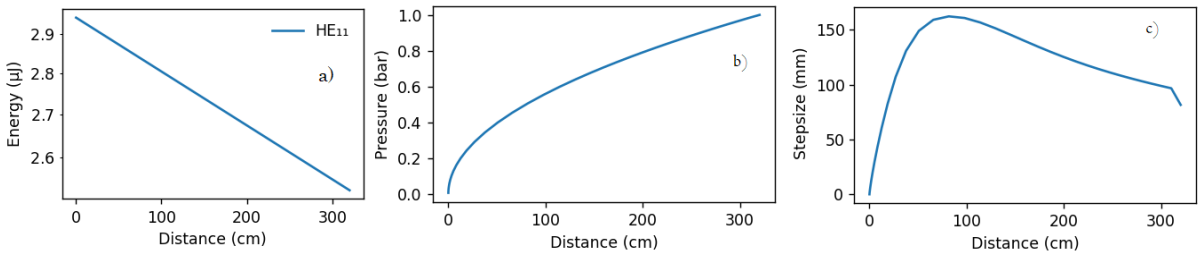


Figure 13: Simulated data of the pulse propagation inside a Neon filled hollowcore fiber
a) Pulse energy against distance inside fiber
b) Pressure inside fiber
c) step size of simulation against distance

The energy of the pulse propagation in the $EH_{1,1}$-mode only drops by about 14 % (see figure 13a) ) along the distance. This is precisely the fiber loss expected for the corresponding mode using the equation 20 and plotted in figure 4, as losses in the transparent gas medium are negligible. As the maximum coupling efficiency is 98.1%, the energy of the pulse propagation does not actually start with exactly 3 mJ in the plot. Figure 13b) shows that the pressure Luna uses along the fiber increases with the distance. This describes the case of a differentially pumped fiber correctly. The stepsize for the splitstep method shown in figure 13 c) shoots up at beginning, then slowly decreases. The necessary step-size is re-estimated by Luna after each step and adapted accordingly in order to optimize the program's performance. Apparently, the step size can reach up to $\sim 1.5$ cm without noticeably compromising the simulation's accuracy. Thus, the numerical error emerging from the simplification of the split-step Fourier method is kept below 0.2 %.

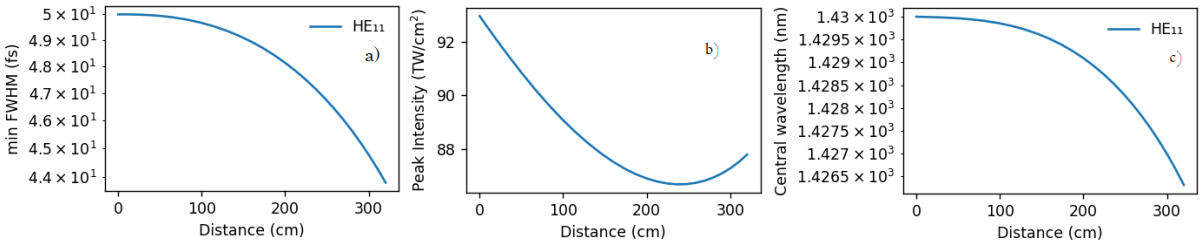


Figure 14: Simulated data of the pulse proagation inside a Neon filled hollowcore fiber
a) FWHM of the pulse duration against distance inside fiber
b) Peak intensity against distance
c) Central wavelength against distance

In figure 14 a), the FWHM if the temporal pulse profile is shown at each position of the fiber, revealing that the nonlinear interaction within the medium reduces the pulse duration. In figure 14 b), the peak intensity at each position is presented. While in this example, the peak intensity is first dropping due to the overall energy losses within the fiber propagation, the reduction in pulse duration increases the peak intensity. After slightly more than 2m of propagation, the peak intensity reaches a minimum and the shortening of the pulse then leads to an effective increasing peak intensity. The central wavelength shown in figure 14c) is nearly stable, but is faintly reduced with increasing distance. This might be due to the asymmetric self-steepening. If the spectrum broadens more in one direction than the other, the central wavelength should shift since it corresponds to the average wavelength of the spectrum.

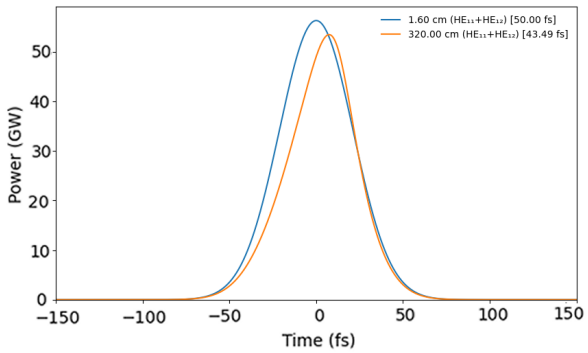


Figure 15: Power against time at the start and at the end of the fiber

The power peak seems to tilt a little to the right with increasing distance. This can be explained by self-steepening, which becomes more pronounced over larger distances.

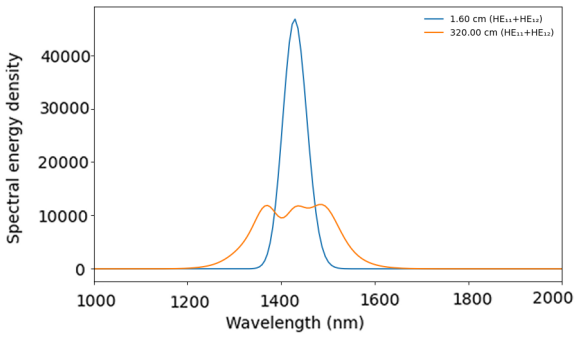


Figure 16: Spectral energy density against wavelength for different distances

As we can see in figure 16[4], the spectrum becomes distinctly broader over longer distances in media. In figure 17, the same information for a continuous range of distances is also presented, as well as the Power's dependency of time and distance. We can see that the spectrum width indeed continuously increases and that the Power continuously shifts to the right with more distance.

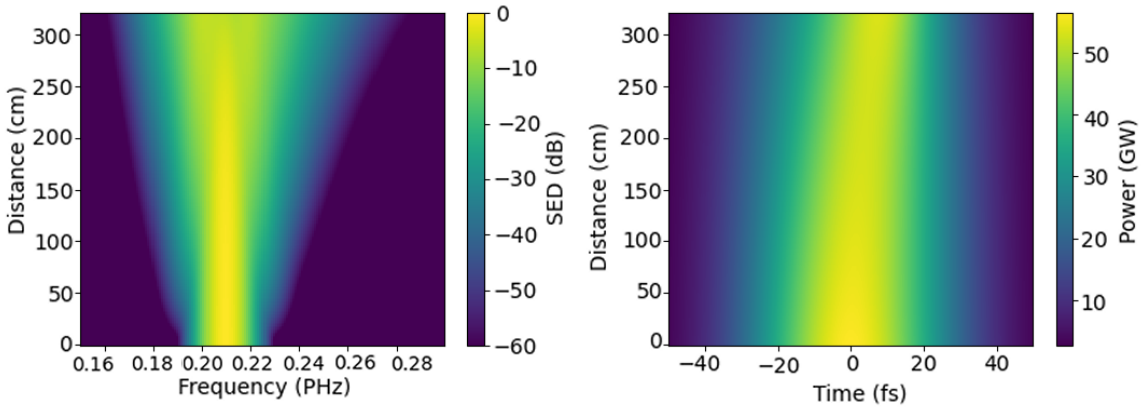


Figure 17: Spectral energy density and power
a) Spectral energy density against frequency and fiber position
b) Power against time and fiber position

### 7.1.1 Varying the input pulse duration

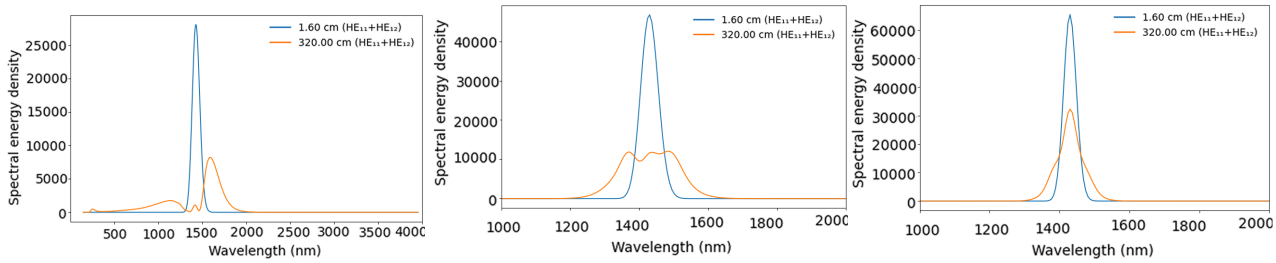


(a) $\tau = 30 \cdot 10^{-15}$ s , note that the range of the wavelength axis is increased here

(b) $\tau = 50 \cdot 10^{-15}$ s

(c) $\tau = 70 \cdot 10^{-15}$ s

Figure 18: Spectral energy density with varying pulse durations $\tau$ at the start and at the end of the fiber

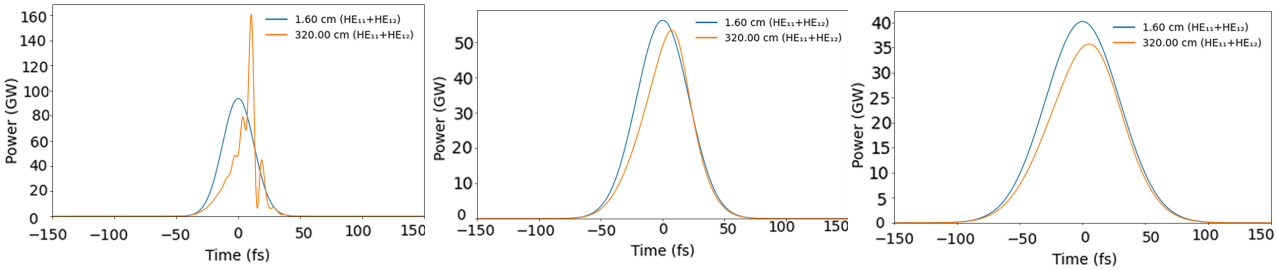


(a) $\tau = 30 \cdot 10^{-15}$ s

(b) $\tau = 50 \cdot 10^{-15}$ s

(c) $\tau = 70 \cdot 10^{-15}$ s

Figure 19: Temporal profile of pulses with different pulse durations $\tau$ at the start and at the end of the fiber

[4]The Jacobi factor is taken into account for.

In figure 18 and 19 the spectral and temporal profiles of Gaussian pulses with different pulse durations are shown, as well as the profiles after propagating through the neon filled fiber. The example of the three different pulse duration with same pulse energy clarifies how the dominant nonlinear effect changes. While the 70 fs pulse mainly shows an almost symmetric broadening of the spectra as expected with the influence of self phase modulation, the broadening of the 30 fs pulse is highly asymmetric.[5]This difference is due to the self-steepening effects becoming more relevant for shorter pulsed duration. Looking at the temporal profile in figure 19 and comparing the plotted pulse before and after the fiber, it becomes evident that the self-steepening effect already plays a role for the 70 fs long pulses, but increases strongly with shorter pulses as the peak is progressively shifted to the right.
To sum it up, figures 18 and 19 display how shorter pulse are affected by the self-steepening effect more strongly, while longer pulses are more influenced by self-phase modulation

## 7.2 Comparison of theory to experiment

The experiment was conducted using the aforementioned Ti:Sa laser, Topas and hollowcore fiber. The pulses used to seed the Topas have an energy of 18.3 mJ, a wavelength of 800 nm and an estimated duration of 30 fs. The idler of 1430 nm ($\widehat{=}$0.87 eV) is used as central wavelength. The overall conversion efficiency of the Topas amounts to approximately 38%, resulting in 3.8 mJ idler pulses.
In order to properly couple the idler beam into the hollowcore fiber, multiple parameters need to be taken into account.
First and foremost, the focal beam waist should correspond to 64% of the core diameter in order to optimize the coupling into the $EH_{1,1}$-mode. This is ensured through adjustments to the focusing of the telescope and analyzing the focus with a beam profiler. The strong attenuation of the beam reduces the risk of damage to the camera. A camera with silicon pixels was used as a beam profiler in this experiment. The band gap at 1.12 eV , which corresponds to 1100 nm, was too high to detect the idler beam directly. Since the idler pulses were short and therefore had a high peak intensity, the second harmonic was generated inside the individual pixels. The SHG resulted in a photon energy of 1.8 eV, meaning the photons could be detected by the camera.
While optimizing the focus with the lens telescope , the beamprofiler measured a $\frac{1}{e}^2$ diameter of 240 $\mu$m. In view of the fact that this value corresponds to $I(r)^2$, the actual diameter must be roughly $\sqrt{2}$ larger and hence about 340 $\mu$m. This is optimal for coupling a Gaussian beam into the $EH_{1,1}$-mode with a 530 $\mu$m diameter.
Secondly, the coupling into the fiber was to be optimized. Thus the signal beam was attenuated to about 0.1 mJ pulse energy as for the power before and after the fiber to be measured with a power meter. The in-coupling position of the fiber was optimized in regard of the beam power at that spot. Furthermore the beam propagation direction had to match the direction of the fiber. This was provided by first aligning the beam without the fiber and then placing the latter along the beam propagation line. Following the coupling into the fiber, the angle could be still slightly adjusted by carefully moving the end of the fiber. Finally the focus position was shifted with the lens telescope so as to guarantee its position at the entrance of the fiber.
The adjustment of all of the parameters mentioned above allowed for a throughput of up to 40%.
Despite this, removing the attenuators and sending the full power into the evacuated hollowcore fiber only left a throughput of about 20%: Minor adjustments to the in-coupling parameters did not significantly improve the transmission. Considering the peak intensity of the focused beam being in the magnitude of $10^{14}$ W/cm$^2$, each major adjustement could be critical and had to be thoroughly examined as the entrance of the fiber was easy to damage. Hence the tests were continued despite the rather low throughput

[5]The broadening would be symmetric as a function of $\omega$. We can already recognize it here, as the Jacobi factor does not make a big visual difference.

of 0.7 mJ−0.9 mJ after the fiber.
The experimental data comes along with quite some uncertainties. The light did not couple into the $E_{1,1}$ -mode properly, a lot less light from this mode got transmitted through the fiber than expected. The transmission rate through the fiber with the attenuated beam is only 40% . This indicates that the Topas' beam is not perfectly Gaussian, as in this case a throughput of about 80% would be expected. The reduced throughput could also be due to the fiber itself. The throughput was also measured using an alignment laser, which resulted in values to up around 80% . Despite the power loss due to the beam's imperfection before the fiber, the output beam has a good Gaussian profile. This shows the fiber acts as a spatial mode filter, since light traveling in higher fiber modes is strongly attenuated.
The more problematic uncertainty of the experimental data comes from the drop of 40% to 20% throughput when changing from the attenuated to the full power beam. In the simplest case, this might be a consequence of insufficient optimization of the coupling after increasing the power, but it might also happen due to some damage at the entrance of the fiber.
These uncertainties imply that we do not know what the true exact starting parameters of our beam inside the fiber are. It is especially unclear how much of the pulse energy actually goes to the $EH_{1,1}$.
In total two measurements were performed: one with argon and one with neon as target gas. In both cases, the fiber was pumped differentially. The backside of the fiber was connected to a gas reservoir with a constant pressure and the front side was evacuated.
In figure 20 the spectra after the fiber for the lowest and highest pressure of each scan is shown for both neon and argon.

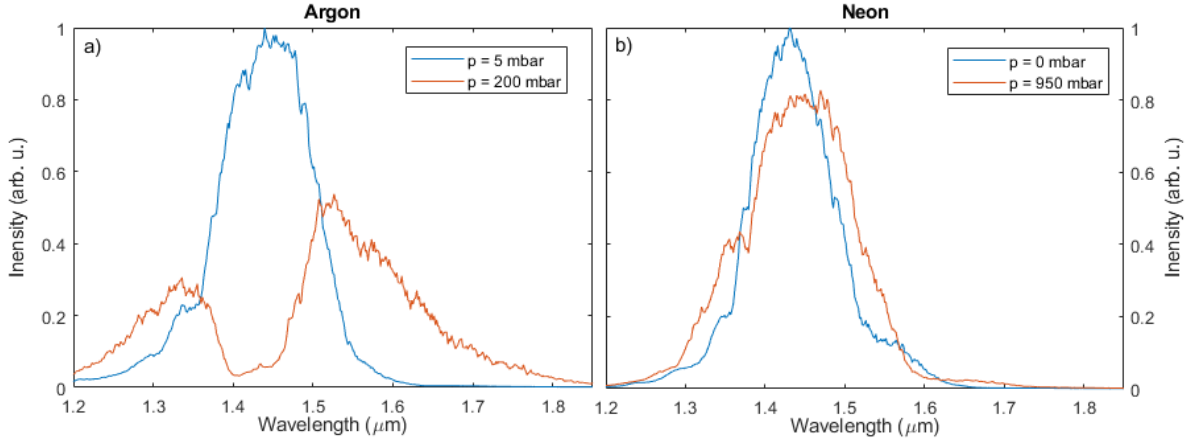


Figure 20: The spectra were measured after the beam's propagation through the 3.2 m long hollowcore fiber. The spectra are displayed for both the lowest and highest pressure in the fiber for a) argon and b) neon.

As can be recognized in figure 20, higher pressures lead to lower intensity peaks in general. In both cases, significant spectral broadening appears. The neon peak for the higher pressure is slightly shifted to longer wavelengths due to the self-steepening effect, as expected (see 9). With argon specifically, the intensity peak gets split up in two peaks surrounding the central wavelength of the initial 5 mbar peak.
As the energy that coupled in the $EH_1$1-mode is uncertain and the argon spectrum seems to become significantly broader in the fiber, I chose argon to conduct several simulations with varying pulse energies. These simulations are meant give a better idea of the coupled in pulse energy in order to estimate it. They are presented in figure 21 next to an experimental measurement.

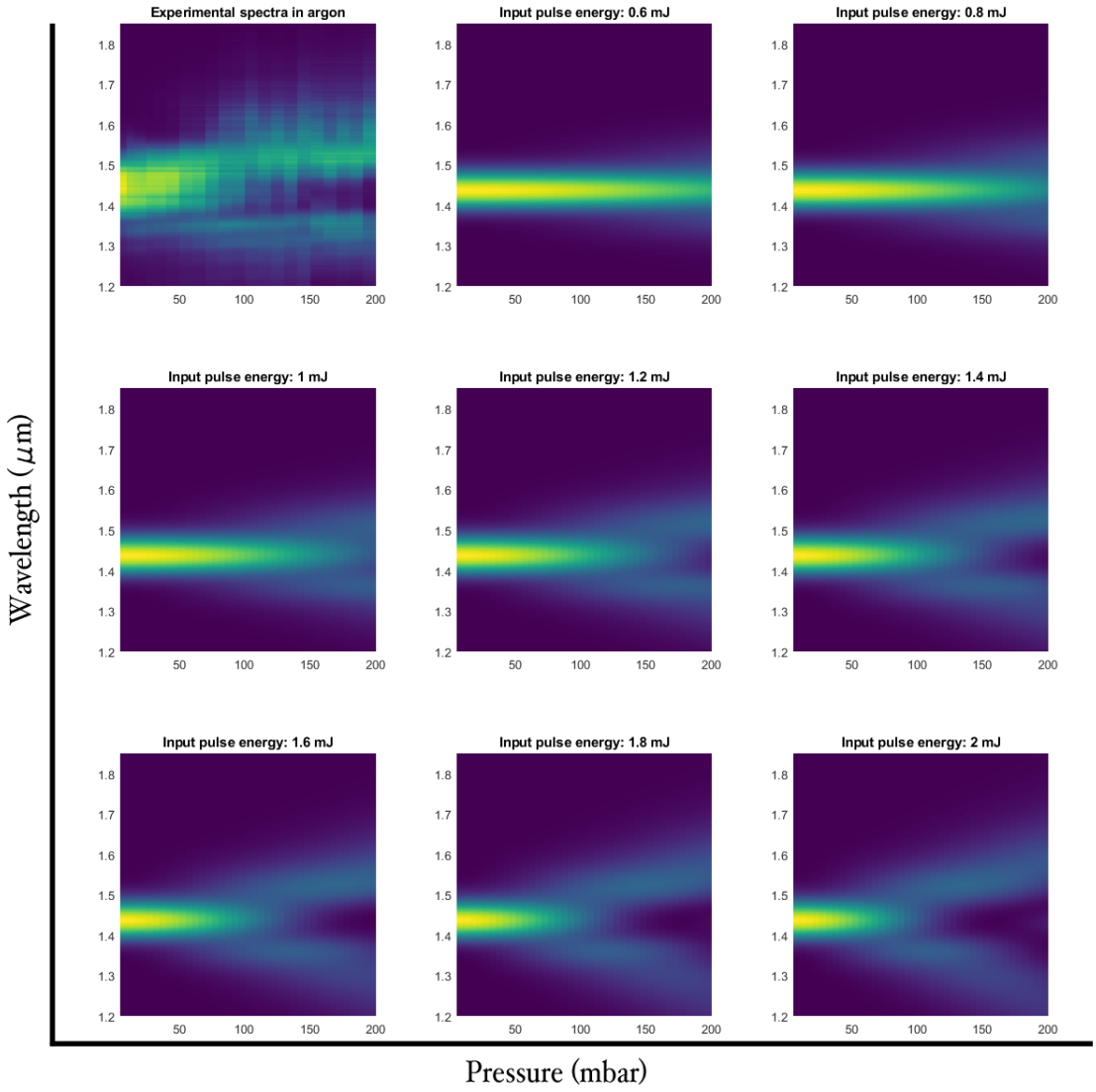


Figure 21: Argon pressure at the end of the fiber in mbar
Experimental spectra of 200$mbar$ argon pressure at the fiber exit compared to simulation results for different energies coupled into the $EH_{1,1}$-mode of the fiber

Figure 21 shows wavelength spectra plotted against pressure for different input pulse energies, as well as the corresponding experimental data. Moreover, given a sufficiently high pulse energy and pressure, the intensity of the spectrum of argon around the main wavelength apparently decreases, creating somewhat of a split. This split becomes clearly visible at a pulse energy of around $\sim 1.2$ mJ.
Since we do not know the input energy of the real pulse we can compare it to simulated data to get a rough idea. Just by looking at the 2D plots, we can already guess it must be above 1 mJ, as the split of the experimental spectrum is well pronounced at 200 mbar.
This becomes more apparent by looking at figure 22, which shows a clearer comparison of the overlayed experimental spectrum and the spectra between 1.0 and 1.4 mJ at 200 mbar. The spectra for this range of pulse energy bear the strongest resemblance to the experimental spectrum. Since the simulation and the experiment match each other roughly, we can estimate that the effective coupled in pulse energy must have been close to 1.2 mJ. This corresponds to only 30% of the pulse's energy before entering the fiber,

implying that the coupling was badly optimized for the full power.

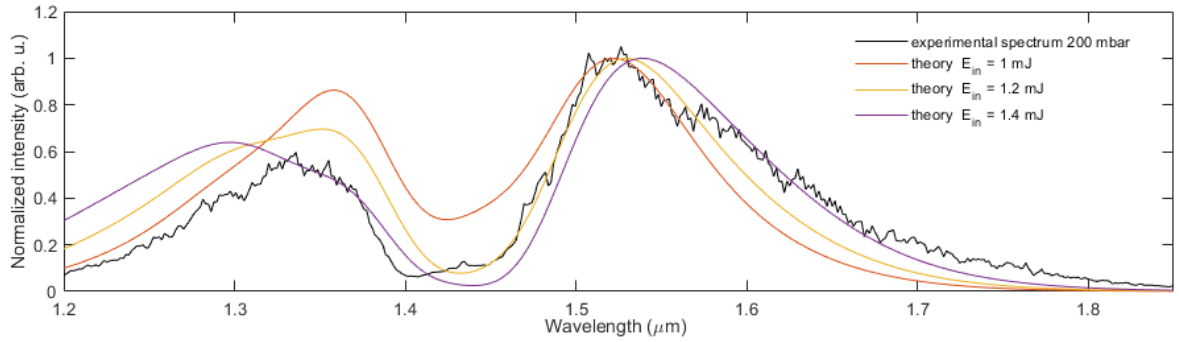


Figure 22: Experimental spectra of 200 mbar argon pressure at the fiber exit compared to simulation results for different energies coupled into the $EH_{1,1}$ mode.

I also plotted the same values for a hollowcore fiber differentially pumped with neon. Once more, the experimental spectrum plotted against pressure is compared to different simulated spectra for varying input pulse energies in figure 23. Here it is harder to discern the fitting input pulse energy, as neon doesn't produce any split in the spectrum, but merely a slight broadening of the spectrum at its tails. This is not very helpful, since the experimental data is already broader than it should be under perfect conditions. Hence, it wouldn't make any sense to plot an equivalent of figure 22, we can't deduce much from this. Still, the rough shape remains recognizable. As we can see, higher pressure combined with higher input pulses energies broadens the frequency spectrum, reducing the peak intensity.

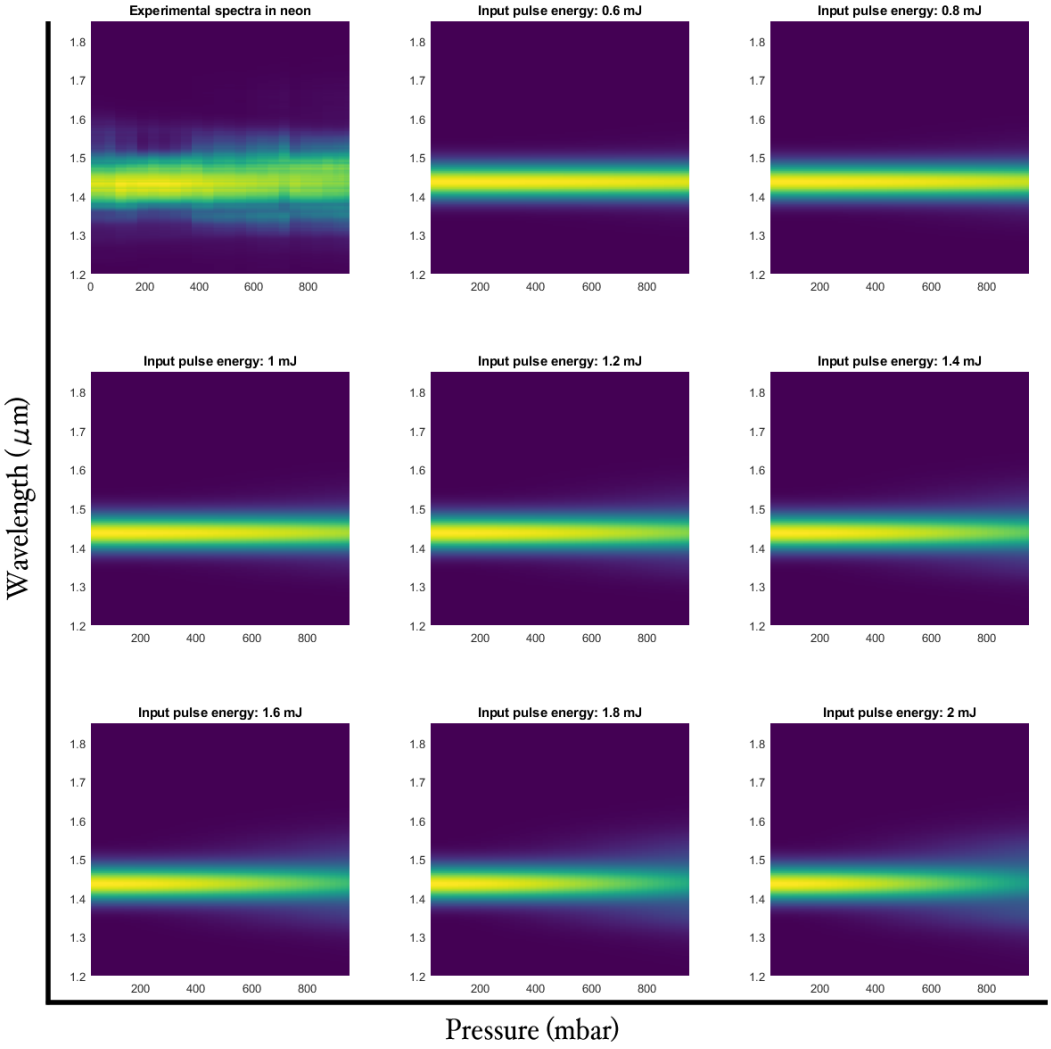


Figure 23: Neon pressure at the end of the fiber in *mbar*

This simulation shows neon is an excellent candidate for spectral broadening, especially for higher coupled in pulse energies (e.g. 3 mJ). For low energies, as used in our experiment, a pressure above 1 bar would likely have been better, but we did not want to subject the fiber to overpressure for the moment, as the whole system was only designed for underpressure.
To sum it up, the comparison shows it is possible to use Luna to simulate the spectral broadening inside a fiber well. In my case, I used the simulation to estimate the coupled in pulse energy. Unfortunately, an exact comparison proved to be difficult due to additional unknown experimental parameters. Aside from the unknown coupled in pulse energy, the pulse duration of 40 fs was only an estimate, as there was no space left in the lab to conduct measurements for that.

## 7.3 Compressing the pulses after the fiber

So far Luna was used to show the spectrum and time dependent intensity for pulse broadening in a fiber. The spectral width at the end of a fiber will help later to create a much shorter pulse than the actual pulse duration at the end of the fiber. The nonlinear effects caused by the propagation through the gas

inside the fiber widen the spectrum, meaning the Fourier limit [6] of the pulse is lowered, enabling shorter pulses. The fiber also adds a chirp to the pulse, bringing the frequencies out of phase. When the pulse exits the fiber, the frequencies can be brought back into phase, thus removing the chirp reducing the pulse duration to its now lower minimum.
In this section an example is shown on how short the pulses can get and how well one can compress the pulses just by using materials with negative GVD.
The example data set computed with Luna represents a differentially pumped fiber with a 530 $\mu$m core diameter, like before. Argon is set as a target gas with a maximum pressure of 100 mBar at the outlet. I chose the input pulses to be Gaussian with a 40 fs pulse duration, 3 mJ pulse energy and central wavelength of 1.3 $\mu$m. The modulations of the spectral and temporal fields amplitude within the 3.2 m long fiber propagation are shown in figure 24. Additionally, the spectral and temporal electric field's amplitudes and phases are shown at the end of the fiber. For this example the spectral phase at the end of the fiber is clearly no longer described well enough only by assuming a chirp, as it also possesses higher order phases.

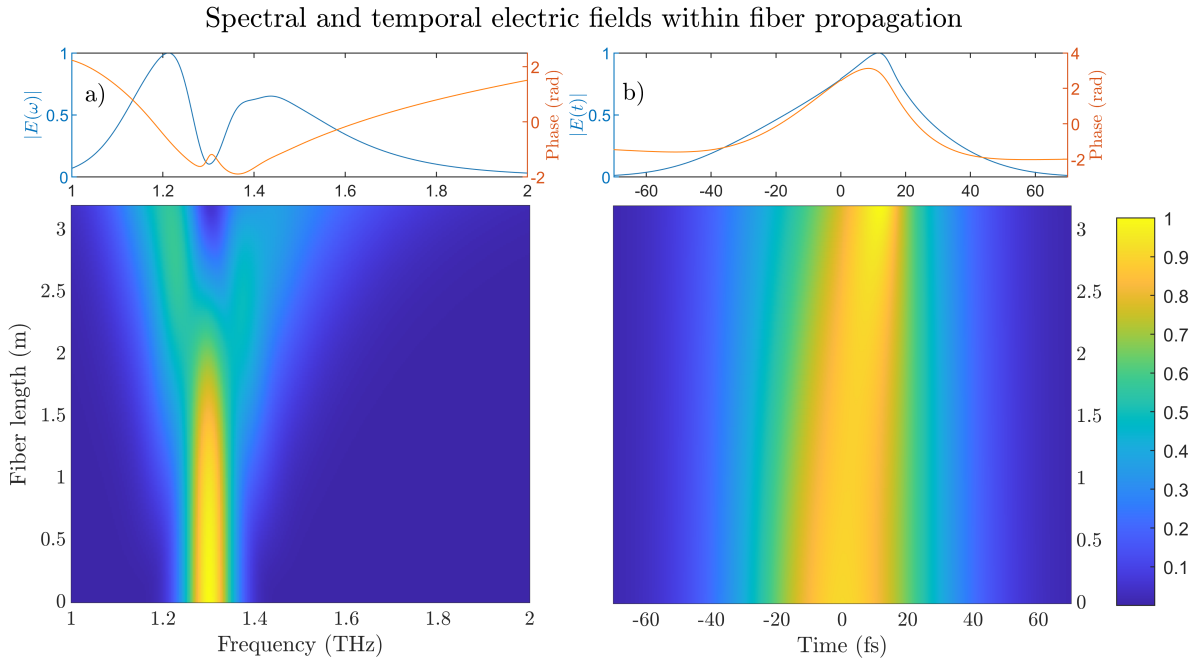


Figure 24: In a) the spectral and in b) the temporal electric field's amplitudes and phases are shown after propagating through the fiber. In the two dimensional plots below the evolution of the amplitudes over the fiber propagation are visualized.

In order to compute the shortest possible pulse that the spectrum allows, one can simply set the spectral phase to zero and Fourier transform into the temporal domain. The resulting pulse is shown in figure 25a). The corresponding intensity profile has a temporal full width half maximum of 7.4 fs. The temporal profile of the pulse is no longer Gaussian as a consequence of the spectral profile being no longer Gaussian. In fact the splitting around the central wavelength in the spectrum leads to pre- and post pulses, but they are far below half of the intensity maximum ($\approx 4\%$).

[6] minimal pulse duration

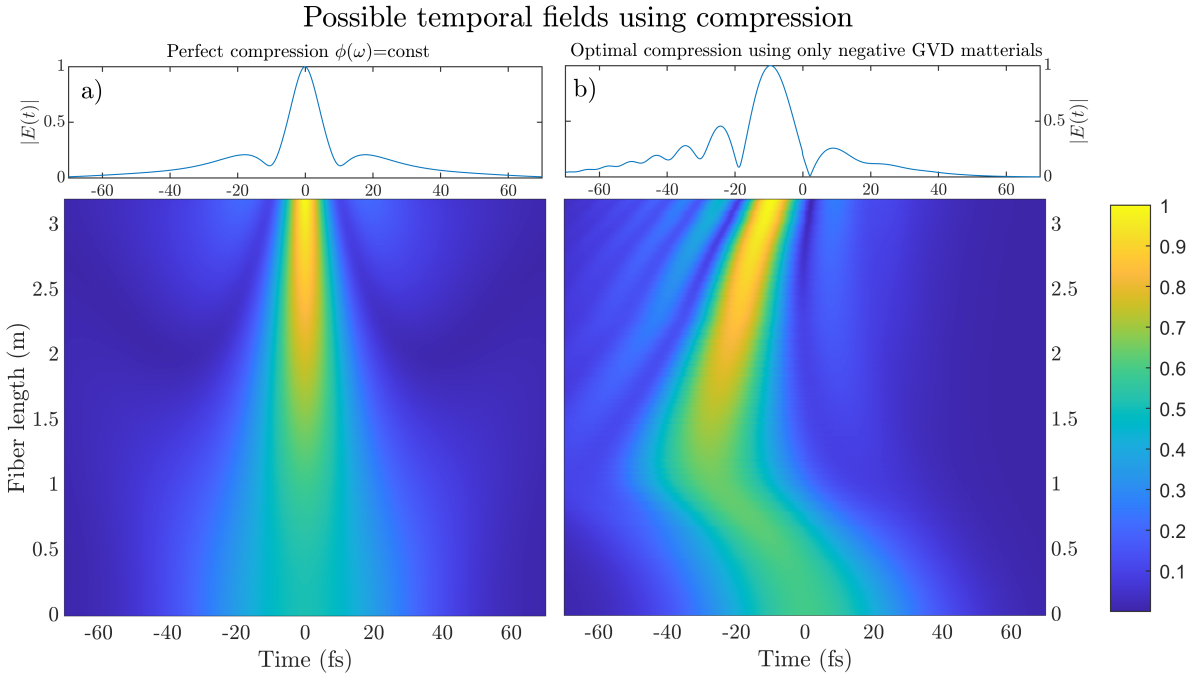


Figure 25: In a) the perfectly compressed pulse of the spectral field in figure 24a) is shown and in b) the shortest possible pulse by only removing a chirp is shown. The two dimensional plots below show the same methods of compression for fields at each position of the fiber.

It is quite difficult to build an experimental setup that can remove an arbitrary phase, as specially designed optics are required here. Nevertheless, as was shown in figure 7, in the near infrared range above 1 $\mu$m wavelength, crystals with a negative GVD do exist. It is therefore rather easy to remove a chirp from the spectrum. The shortest temporal field can be achieved by removing a quadrature phase, as is shown in figure 25b). The corresponding intensity profile full width half maximum is 9.8 fs, and is therefore only 30% longer than in the case of perfect compression. In total, more energy is present in the pre- and post pulses but it is still rather low compared to the main pulse. The most pronounced post pulse has about 20% of the intensity of the main peak. This example demonstrates one advantage of working with longer wavelengths than the commonly used Ti:Sa wavelength (800 nm), as compression can be achieved by for example simply placing an ADP crystal of the right thickness.

## 7.4 Testing models beyond the GNLSE

Luna grants the possibility to compute the interaction of strong laser pulses with media in several ways. So far we have used the envelope mode with the Kerr response, which solves the GNLSE with SPM and self-steepening as nonlinear effects resulting in spectral broadening.

On a different note, it is interesting to consider other physical effects which can appear in real fibers, but that were not considered so far in our GNLSE. The most important yet undiscussed effect is the generation of odd harmonics in the medium and the ionization of the medium.

To the best of my knowledge, those effects cannot be included into the GNLSE as the full field, including the carrier, would need to be taken into account for. In this section, other functions of Luna are used to apply different models allowing for a qualitative example on how third harmonic generation and ionization effects would affect the output with spectral broadening in a fiber.

Let us briefly introduce the model used by Luna. Since the full electric field must now be considered, the

forward Maxwell equation, which can be deduced from nonlinear wave equation 36, is used.[7] Concerning the nonlinear polarization, Luna can again take the Kerr-effect into account in its calculations. Additionally, the third harmonic generation can be implemented as the dominant frequency for the up-converting process inside the noble gas target. It can also be considered for rather high field intensities ionization using the PPT model. [18].
In order to test the full field model, it can be compared to the envelope model used previously. Short pulse propagation inside of an argon filled fiber is computed in both cases with solely the Kerr effect taken into account amongst the nonlinear effects. The two resulting spectra are displayed in figure 26 and show the outcome is identical. Only in the low frequency region, where nearly no intensity remains in the spectrum, does a small mismatch emerge due to the differing numerical implementations.

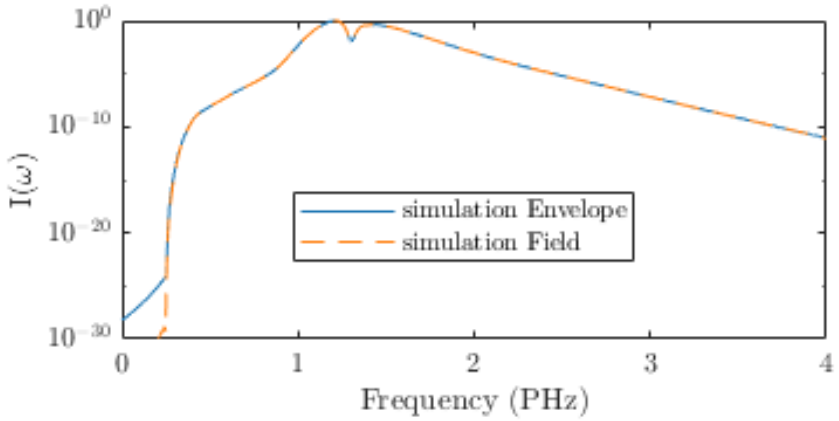


Figure 26: Comparison of the simulations in the fiber using the envelope model (GNLSE) and a full field model.

Two examples are provided in figure 27 to test the effects of including third harmonic generation and ionization in the propagation. In each case, 40 fs input pulses with a Gaussian envelope and a 1.3 $\mu$m central wavelength are used and are propagated through a 3.2 m long hollowcore fiber which is pumped differentially with 100 mbar pressure at the outlet with argon. In figure 27 a) and b) the input pulse energy is set to 1 mJ. The models including and excluding ionization show no major differences for this case and I therefore did not plot them.
The spectra of the linearly scaled plots (figure 27 a)) are clearly broadened at the tails compared to a Gaussian profile. This broadening is mainly symmetric. Otherwise the spectra including the THG look nearly identical.
Only if plotted logarythmically (figure 27 b) ) does the difference become obvious. Where for including THG a peak at three times the fundamental frequency, the third order harmonic is clearly visible for THG, as the peak corresponds to thrice the fundamental frequency. Additionally a small peak at the fifth harmonic frequency appears, despite the fact that nonlinear effects caused by susceptibilites above the third order were not included. The emergence of the fifth harmonic is caused by a combination of a third harmonic photon and two fundamental photons ($5\hbar\omega = 3\hbar\omega + 1\hbar\omega + 1\hbar\omega$). This only happens after a certain propagation time, as the third harmonic frequency becomes unnegligible in the spectrum. The aforementioned three photon process is also described by third order susceptibility.
For this first example the effect of including the THG is rather irrelevant as only a small fraction of $3 \times 10^{-4}$ of the intensity is converted into the third harmonic.
In the second example the pulse input energy is increased to 3 mJ. This roughly corresponds to the highest intensity that one can expect to couple into the hollowcore fiber with our laser and TOPAS setup. In this case THG as well as ionization has an effect on the linearly plotted spectrum (figure 27 c)).

[7] For more details see [6].

When THG is included, the spectrum is to be slightly less broadened and is a little more intense within the central part of the spectrum. This is most likely due to the nearly 1% intensity loss caused by the THG process and the consequently reduced fundamental field intensity, resulting in slightly less SPM and self-steepening. With the three times higher input field and the exponentially increasing strong field ionization, ionization is also no longer negligible. For both spectra that include ionization with and without THG, the peak in the higher frequency range is clearly more pronounced compared to the spectra with neglected ionization. The lower frequency peak is also less intense and up-shifted. The ionized gas causes the plasma blue shift to appear.
Testing the additional models clearly shows that due to the non-linearity of all considered effects, a change of the input energy by a factor of three already clearly compromise the precision of the GNLSE to correctly describe all important effects appearing in the fiber. Here ionization in particular leads to the strongest changes.
To obtain better experimental results when dealing with higher input pulse energy, one can easily increase the fiber diameter, resulting in a lower peak intensity and therefore ionization. One could also simply change the gas used within the fiber to neon. With an ionization energy of 21.6 eV in neon compared to argon with 15.6 eV, the amount of ionization taking place is magnitudes lower in neon and is therefore negligible for the simulations.

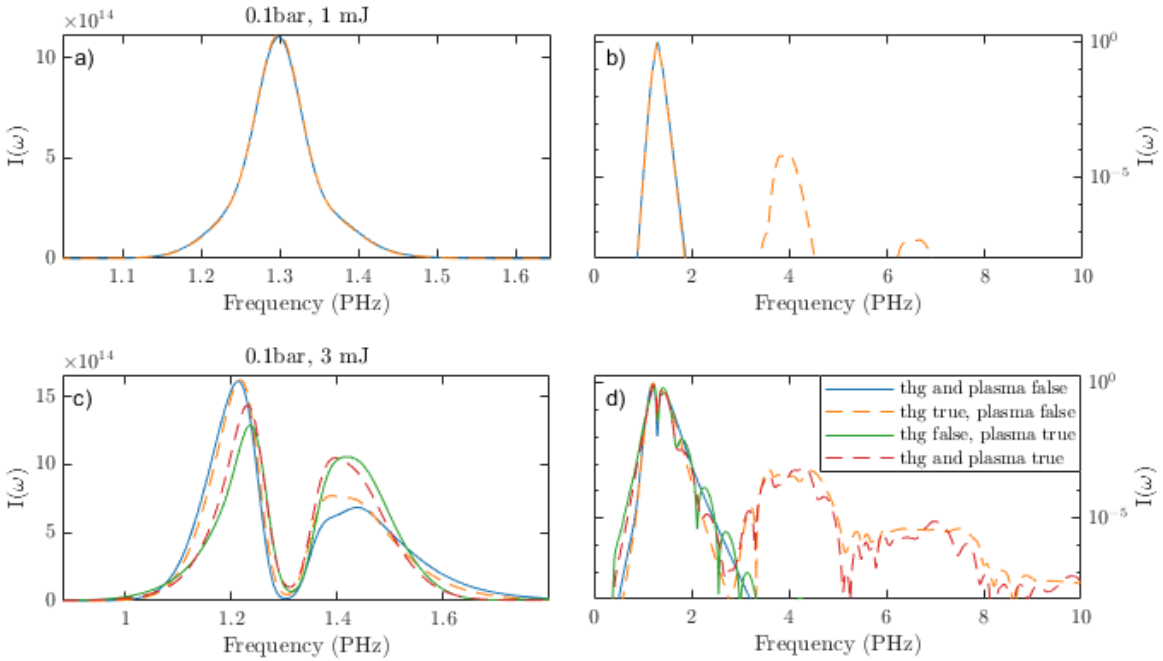


Figure 27: Different physical models for simulating propagation within an argon filled hollowcore fiber of 40 fs pulse with Gaussian envelope and 1.3 $\mu$m central wavelength. All models include the Kerr-Effect. In a) and b) the pulse energy is 1 mJ and the model only including and excluding third harmonic generation are compared. In c) and d) the pulse energy is 3 mJ and models with and without third harmonic generation and ionization (Plasma effects) are shown. b) and d) are normalized to the highest accrued intensity.

# 8 Sources

# References


[1] Accessed on 05.11.2023. URL: https://mathworld.wolfram.com/BesselFunctionZeros.html.

[2] A Börzsönyi et al. "Dispersion measurement of inert gases and gas mixtures at 800 nm." In: Applied optics 47.27 (2008), pp. 4856–4863.

[3] Robert W Boyd, Alexander L Gaeta, and Enno Giese. "Nonlinear optics." In: Springer Handbook of Atomic, Molecul Springer, 2008, pp. 1097–1110.

[4] Christian Brahms and John C. Travers. Luna.jl. DOI: 10.5281/zenodo.5513570.

[5] Nobel Foundation. The Nobel Prize in Physics. Accessed on 01.10.2023. 2018. URL: https://www.nobelprize.org/prizes/physics/2018/summary/.

[6] Anton Husakou. "Nonlinear phenomena of ultrabroadband radiation in photonic crystal fibers and hollow waveguides." PhD thesis. Free University of Berlin, 2002.

[7] T. W. Kelly et al. "Gas-induced differential refractive index enhanced guidance in hollow-core optical fibers." In: Optica 8.6 (June 2021). Accessed on 27.10.2023, pp. 916–920. DOI: 10.1364/OPTICA.424224. URL: https://opg.optica.org/optica/abstract.cfm?URI=optica-8-6-916.

[8] Jan Kilinc. "Charakterisierung der nichtlinearen Pulspropagation in einer gasgefüllten Hohlfaser." Ruprecht-Karls-Universität Heidelberg, 2017.

[9] Ian H Malitson. "Interspecimen comparison of the refractive index of fused silica." In: Josa 55.10 (1965), pp. 1205–1209.

[10] Irving H Malitson. "A redetermination of some optical properties of calcium fluoride." In: Applied Optics 2.11 (1963), pp. 1103–1107.

[11] Charles R Mansfield and Edson R Peck. "Dispersion of helium." In: JOSA 59.2 (1969), pp. 199–204.

[12] O. Melchert. Nonlinear Schrödinger equation with loss. Accessed on 05.11.2023. URL: https://omelchert.github.io/py-fmas/auto_tutorials/attenuation/g_NSE_absorption_constant.html.

[13] Marcus R.A. Newman. Self-phase modulation. Accessed on 2.11.2023. URL: https://prefetch.eu/know/concept/self-phase-modulation/.

[14] Marcus R.A. Newman. Self-steepening. Accessed on 2.11.2023. URL: https://prefetch.eu/know/concept/self-steepening/.

[15] M. Nisoli, S. De Silvestri, and O. Svelto. "Generation of high-energy 10-fs pulses by a new pulse compression technique." In: Conference on Lasers and Electro-Optics. Accessed on 09.10.2023. Optica Publishing Group, 1996. URL: https://opg.optica.org/abstract.cfm?URI=CLEO-1996-CTuR5.

[16] Rick K. Nubling and James A. Harrington. "Launch conditions and mode coupling in hollow-glass waveguides." In: Optical Engineering 37 (Sept. 1998). Accessed on 27.10.2023, pp. 2454–2458. DOI: 10.1117/1.601768.

[17] Edson R Peck and Donald J Fisher. "Dispersion of argon." In: JOSA 54.11 (1964), pp. 1362–1364.

[18] A M Perelomov, V S Popov, and M V Terentev. "IONIZATION OF ATOMS IN AN ALTERNATING ELECTRIC FIELD." In: Sov. Phys. JETP 23 (1966), pp. 924–934.

[19] Properties of KDP, DKDP and ADP Crystal. Accessed on 25.10.2023. URL: https://www.unitedcrystals.com/KDPProp.html.

[20] Claude Rullière. Femstoseconds Laser Pulses. 2nd ed. Springer New York, NY, 2004. ISBN: 978-0-387-01769-3. DOI: https://doi.org/10.1007/b137908.

[21] Patrick Dominik Rupprecht. "Ultrafast Laser Control of Molecular Quantum Dynamics from a Core-Electron Perspective." PhD thesis. Ruprecht Karl University of Heidelberg, 2022.

[22] W. Sibbett, A. A. Lagatsky, and C. T. A. Brown. "The development and application of femtosecond laser systems." In: Opt. Express 20.7 (Mar. 2012). Accessed on 03.10.2023, pp. 6989–7001. DOI: 10.1364/OE.20.006989. URL: https://opg.optica.org/oe/abstract.cfm?URI=oe-20-7-6989.